Molecular Dynamics Approach to Mica Surface Reconstruction

by

©Muyi Ant Xu

A Thesis submitted to the School of Graduate Studies in partial fulfillment of the requirements for the degree of

Master of Science

Computational Science/Scientific Computing

Memorial University of Newfoundland

May 2014

St. John's Newfoundland

Abstract

Mica has a layered silicate sheet structure and is widely used as a substrate for imaging biological samples. Due to its high thermal stability and negatively charged features, it is interesting to investigate whether the mica substrate will affect sample surface structure by enabling interactions between biological systems.

In particular one has to consider the interactions of fluid or environmental water as well as associated ions with mica itself. Experimentally, previous research group members have observed protein alignment on the mica surface in register with underlying crystal directions. In particular, it is not clear how the protein and mica structures are connected across several length scales. We apply molecular dynamics (MD) calculations to investigate whether the mica substrate affects ordering of the ions in water. We first optimize the mica structure with four K^+ ions originally in the system. Then we use two methods to check whether ions effect the mica surface reconstruction. The two methods are: replacing K^+ ions with Na^+ ions and removing ions from the mica system.

Our calculations show that K^+ and Na^+ ions induce different surface reconstruction of mica. Furthermore, ion arrangements on the mica surface play an important role in water pattern formation. In this way, the nanoscale crystallographic reconstruction of the mica surface may be translated into a micro-scale pattern for protein alignment.

Acknowledgements

I, first and foremost, would like to give my utmost gratitude to Dr. Erika Merschrod for giving me the opportunity to obtain my master degree in the Computational Science program in Chemistry under her supervision. Her encouragement, guidance and support from the initial to the final level enabled me to develop an understanding of my first computational research project and has been my inspiration as I overcome all the obstacles in the completion of this research work. Dr. Erika Merschrod made my research experience extremely rewarding. One simply could not wish for a better or more knowledgeable advisor. I cannot thank her enough for all of her support.

Thanks also to Dr. David Morgan and Dr. Galina Orlova, who introduced me to the chemistry research experience and computational chemistry at STFX university. They inspired me to think deeply about how to learn and to inquire me to challenge myself to explore the experimental chemistry and transfer the theoretical information to a computational chemistry methodology.

Thanks to Dr. Ivan Saika-Voivod, who introduced me to the computational knowledge, gave me the general ideas of how to compile and make files.

Many thanks also to the group of Dr. Erika Merschrod, who truly challenged me and gave me a brand new way to thinking about chemistry. This inspired the transformation from the student I was to the student I have now become. I hope to carry this passion into every endeavour that I undertake.

Sincere thanks to Shaheen Fatima, who became my close friend through our moments of sharing the computational research ideas together and who gave me advice to improve my research. I would like to wish her the best of luck.

Meanwhile, I would like to thank Hao Ling, who helped me debugging and introduced me to computer languages and scripts, and who truly supports me and leads me to the C++ world.

Finally, I would like to thank my entire family who have always believed in me and supported my decisions. They have always wanted me to be happy and wish me nothing but success. I deeply appreciated them allowing me to realize my goals in life, supporting my dream to study in a different country and gaining the experience.

I wish all the best of luck in the future to the graduating chemistry and physics class; I have greatly enjoyed our time together in lectures, labs and in social gatherings.

Thanks also to Memorial university of Newfoundland, Compute-Canada, NSERC, ACEnet and again, my supervisor: Dr. Erika Merschrod for funding.

Table of Contents

List of Tables

List of Figures

Chapter 1

Introduction

Originally people treated mica as a waste product from mining [1], while now mica is used in many applications. Due to its stability and transparent properties, mica is used as a substrate for imaging biological samples [2]. The mica which is being analyzed in this research project is called Muscovite mica [3].

Previously, researchers chose mica as an atomic force microscope (AFM) imaging substrate. Using experimental methods, they found that ions, proteins and mica show alignment of layers [4]. In order to understand the interactions between ions and the inorganic mica substrate, computational simulations are applied. This chapter gives a general introduction of the mica structure and the theory of molecular dynamics simulations, as well as the motivation of our research.

1.1 Muscovite Mica Structure

Mica has a layered silicate structure, as seen in Figure 1.1. In muscovite mica, silicon atoms form tetrahedral structures bonded with oxygen atoms; extra oxygen bonds connect with Al^{3+} [5]. The surface of the layers is oxygen-terminated; the negatively charged oxygens can bind with protons or cations, leaving a neutralized or even posi-

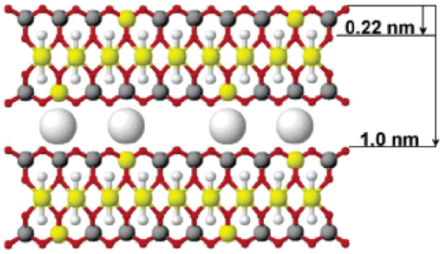

Figure 1.1: Schematic of muscovite mica crystal structure showing oxygen-terminated layers. Large white spheres represent K; yellow: Al; gray: Si; red: O; small white spheres: H. [8]

tive system [5]. These charged surfaces can influence biological adsorbates and overall sample structure, as seen experimentally [4] and computationally [6, 7].

1.1.1 General Crystal Structure

A crystal can be represented by a unit cell and a lattice. The lattice extends in three dimensions and has infinite lattice points. For lattice points, they either stand for one atom or several atoms. Atoms repeat in a certain pattern to form a crystal structure. The unit cell is the repeating unit for the lattice. The smallest and the most simple repeating unit for the crystal structure is the primitive unit cell [9].

Muscovite mica has a monoclinic crystal structure with $C2/m$ symmetry, where C means that the space group lattice is centred on a face, and $2/m$ means a two-fold rotation axis perpendicular to a mirror plane. Atoms are positioned in the unit cell box and have a mirror plane in the centre of the box. The lengths of the three edges of the unit cell are not equal, and the angles between the axes generating the lattice are not all right angles (one is bigger than 90°), as summarized in Table 1.1 [10].

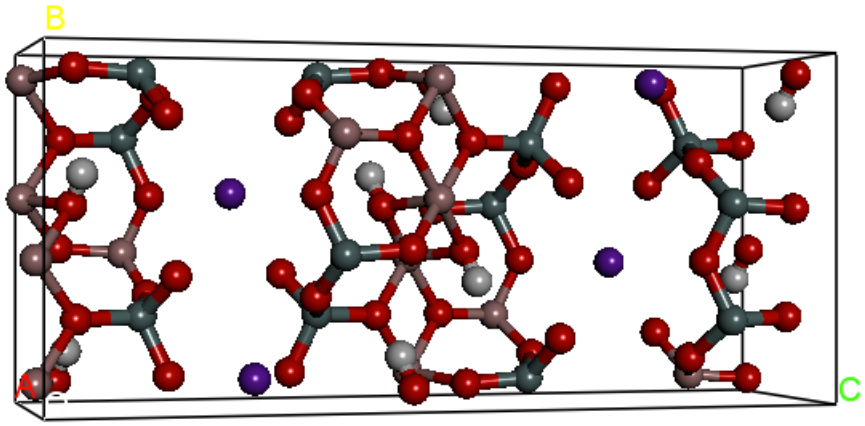

Figure 1.2: Unit cell for muscovite mica with a, b and c axes labeled. Because of rotation between adjacent aluminosilicate layers, the crystal structure contains two aluminosilicate layers which are otherwise identical.

Parameters	Value
a	5.1988 Å
b	9.0266 Å
c	20.1058 Å
α	90°
β	95.782°
γ	90°

Table 1.1: Mica Unit Cell Crystal Structure Parameters [10]

1.1.2 Compositional Variations

The mica group is a group of sheet silicate minerals. Chemically, mica can be written as this formula: $X_2Y_{4\text{-}6}Z_8O_{20}(OH/F)_4$, where X is K, Na or Ca; Y is Al, Mg, or Fe; and Z is Si or Al [11]. With different compositions, mica has different characters and properties, with different names such as biotite, phlogopite, and muscovite.

Muscovite mainly contains aluminum, potassium, silicon and oxygen atoms. Aluminum and silicon have almost equal elements in mica; potassium ions, although fewer in number, play an important role. In this research, the model formula is $K(Si_3AlO_8)(Al_2O_2(OH)_2)$ [3, 5].

1.1.3 Reconstruction of Mica Surface

Atoms at a surface have different properties than those in the bulk due to the forces they encounter. When atoms are in the bulk, they have forces coming from all directions leading to a particular equilibrium arrangement. At the surface, atoms do not have the same inter-atomic forces from both directions compared with those atoms in bulk. The imbalanced forces make the surface atoms migrate to produce a new layout. The new pattern does not have the same atom spacing in comparison with the bulk.

Because mica has a layered structure, it cleaves naturally to expose (001) planes [12]. The atoms exposed on these planes, particularly the potassium cations, can move to change the structure of the top layer or layers. Mica should have oxygen-terminated flat surfaces in theory, as depicted in Figure 1.1, but the true surfaces can change, particular in the presence of ions and water [13]. Figure 1.3 shows a top view of the mica (001) reconstructed surface: the oxygens are more tilted rather than staying on a layer. The light circles are oxygen atoms above the plane, the dark circles

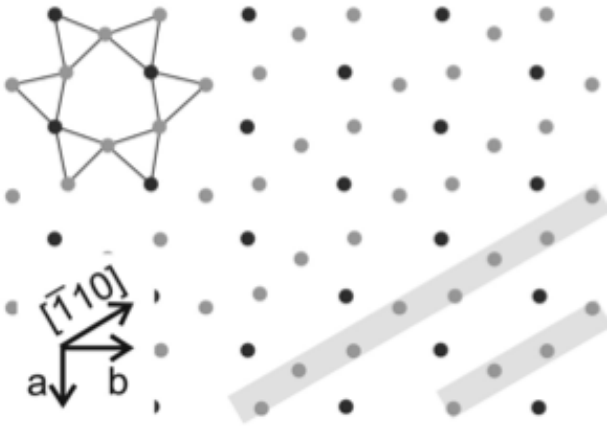

Figure 1.3: Schematic of the proposed mica (001) reconstructed surface [4].

are oxygen atoms below the plane. In my research, I am mainly focus on the mica surface reconstructions.

1.2 Mica as an Imaging Substrate

Mica is a widely used substrate for imaging biological samples with an atomic force microscope(AFM). Atomically-flat planes can be prepared by simply removing a layer using adhesive tape [14].

The mica surface is ionic, and fluid or environmental water are associated with these ions. Biological systems are often imaged in fluid, which is therefore also interacting with the mica surface. But even without the intentional inclusion of liquid water, there is always a layer of water on the mica from the surrounding environment unless working under vacuum. This water layer can impact the mica surface structure as well as its interactions with other adsorbates being imaged.

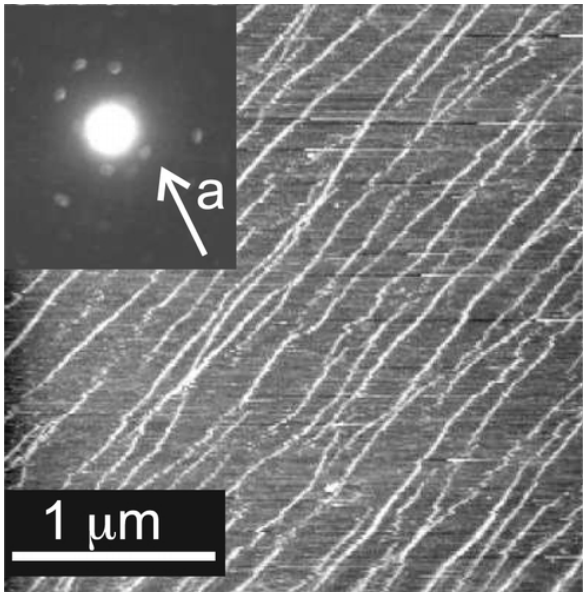

Figure 1.4: Protein microfibrils on mica showing alignment with underlying mica crystal orientation (inset)[4].

1.2.1 Biological Samples on Mica Imaged by AFM

There are many examples of AFM imaging of biological systems with mica as a substrate, and within that literature there are a number of cases where the mica substrate influences the biological sample. For example, researchers put different concentrations of nucleotide (GMP) solutions on mica surfaces and found that the ions on the mica surface induce self-assembled aggregates of the adsorbates [15].

Previous research group members put collagen (a protein) on top of the mica surface and detected that the collagen-mica system forms patterns spontaneously. They concluded that collagen has some interactions with mica [4]. Figure 1.4 [4] shows the AFM image of the protein microfibril pattern along with the X-ray diffraction pattern from the underlying mica, indicating the co-orientation of the two layers.

1.2.1.1 Water on Mica Imaged by AFM

Figure 1.5 [16] shows a water covered mica surface structure obtained by AFM in contact mode. (Panel a is the raw data; the other panels show images after filtering.) Researchers cleaved the muscovite mica surface and immersed it in water. Water drives mica surface rearrangement, as the re-arrangement of the hexagonal rings of SiO_4 tetrahedra was observed.

The AFM image in Figure 1.5 shows the arrangement of the hexagonal rings of SiO_4 tetrahedra [16]. After immersing mica in water, the arrangement gradually changed. By measuring the mean unit cell dimensions for the mica surface, researchers found that the re-patterned structure gives slightly longer unit cell dimensions (a = 5.28 Å, b = 9.28 Å) than for the bulk structure (a = 5.1988 Å; b = 9.0266 Å). Researchers deduced that the water interacts with the mica surface, causing some structural relaxation of the tetrahedral sheet surface.

1.3 Modelling Mica

So far, researchers have studied cation energetics exchange from one mica layer to another layer using density functional theory (DFT) with plane-wave pseudo-potential. They compared the initial and final states of the Cs/K exchange in the mica interlayers, to conclude that cation exchange in mica is a favoured process due to the small amount of energy consumed [17].

Also Molecular Dynamics (MD) simulation was used to calculate the liquid water absorption on mica surfaces. A series of MD calculations were used for checking water absorption (water amount) on the mica surface under the same NVT conditions with different time lengths [18]. By comparing with X-ray measurements and checking the water angle with respect to mica layers, researchers found out that increasing the

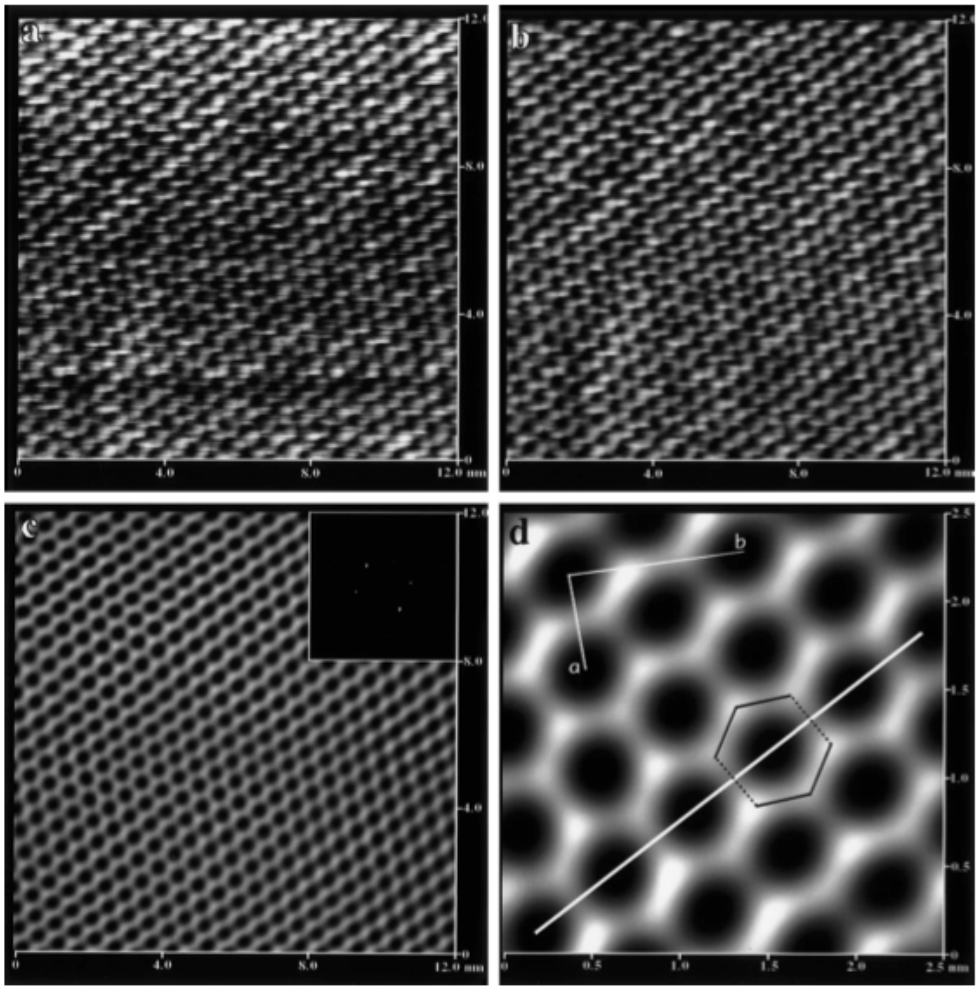

Figure 1.5: AFM image of a mica surface exposed to water [16].

water thickness on top of mica would not make a big difference; hydrogen bonding plays an important role of water absorption on mica surface [18].

1.3.1 Modelling Water and Ion Adsorption on Mica

MD simulation was carried out for analyzing the absorption of an aqueous film on the surface of ammonium substituted mica [19]. From the calculations, researchers found that when the aqueous water layers get closer to ammonium ion-substituted mica, hydrogen bonding occurs [19]. Another MD calculation was intended to check interfacial behaviour of water bonding (hydrogen bonding) and water orientation by varying the interfaces from strongly hydrophilic to strongly hydrophobic [18]. Water with vapor, talc (001) and mica (001) interfaces were checked, and different local environment makes a difference in water adsorption [18]. Also, water preferences change obviously during the interactions of hydrophobic and hydrophilic surfaces [18].

Due to the important role water adsorption plays on solid surfaces, many water-ions experiments can be carried out to check water surface properties. For example, Monte Carlo simulations of water on mica surface were run, varying the arrangement and concentration of potassium ions. The water and air interfaces were observed; by increasing the concentration of ions, the water film locates around the same positions as detected experimentally by SPFM (scanning polarization force microscopy) [20]. Ab initio molecular dynamics studies of monolayer, bilayer, and trilayer water adlayers on the muscovite mica (001) surface were also checked [21]. Researchers found that strong hydrogen bonds were formed for water molecules. Oxygen on the mica surface, bridging with the closest water molecule layers, formed a low diffusion interface. Different layers of water have different properties and the simulation results were consistent with AFM experimental images [21].

1.4 Molecular Dynamics Simulations

In this research, molecular modelling is performed by adding molecules and ions and allowing bond lengths and intermolecular distances to vary.

With the fast development of the computer, computer simulations have been carried out as a new technique to explore science. The first computer simulation carried out at the time of World War II, to create nuclear weapons. Monte Carlo simulation was used to make accurate calculations of the power of weapons, which was impossible to be done by experimental methods [22]. Later, many simulations methods have been developed, such as Molecular Dynamics (MD) simulation.

MD simulation can compute equilibrium and transport properties for a system[23]. First and foremost, MD simulation follows Newton's laws of motion: $F = ma$. Also, in the calculation, MD simulations can obey the requirements researchers give as input. For example, initial atoms' velocities, system's pressure and atom coordinates can be provided as data files. At each time step, the calculation generates results such as total energy of the system. MD methods are good for thermodynamic calculations [23]. In this research, MD simulations are carried out to investigate average equilibrium system features rather than dynamics.

1.4.1 General Principles

MD obeys classical mechanics laws, which is a good approximation and cost-effective for large systems, particularly when studying non-covalent interactions. During the calculation, certain conditions, such as temperature, system volume, pressure, molecules' velocities can be set or changed as the time steps vary. After the system of interest reaches its equilibrium, researchers can perform further measurements on structure and properties. In order to measure the properties in a MD simulation, we can express

this observable as a function of the positions and momenta of particle in the system [23].

Researchers need to initialize the parameters of each run, such as the number of particles in the system, reasonable bond distances of the neighbouring atoms, and temperatures or pressures for the run. To start a simulation, the initial coordinates of all particles in the system should assigned close to the reality. For example, particles should not be positioned within bonding distance causing the overlapping of molecules with each other; bond lengths between two atoms are supposed to be approximately the same as the experimental data.

A general form for inter-particle interactions is the Lennard-Jones potential, where ϵ is a parameter governs the strength of the interaction and some length scale terms. For a Lennard-Jones system (in reduced units), force ($f(r)$) can be represented as: [23]

$$f(r) = \frac{48\epsilon}{r^2}\left(\frac{1}{r^{12}} - 0.5\frac{1}{r^6}\right). \tag{1.1}$$

The cut-off energy e_{cut}, is an arbitrary minimal potential energy value, occurring at $r = r_c$, where r_c is the cut-off radius. The cut-off energy is shown below [23]:

$$e_{cut} = 4\left(\frac{1}{r_c^{12}} - \frac{1}{r_c^6}\right). \tag{1.2}$$

1.4.1.1 Periodic Boundary Conditions

Periodic boundary conditions (PBC) are used. PBC are suited for a large system, by setting a boundary in order to turn a big simulation into repeated small calculations of atoms or molecules [24]. To let a small system represents a big simulation, researchers assume that when an object passes through one face of the small system, it reappears on the opposite face with the same velocity and position. In general, the periodic boundaries can be larger than the smallest unit cell of the system, where the repeat

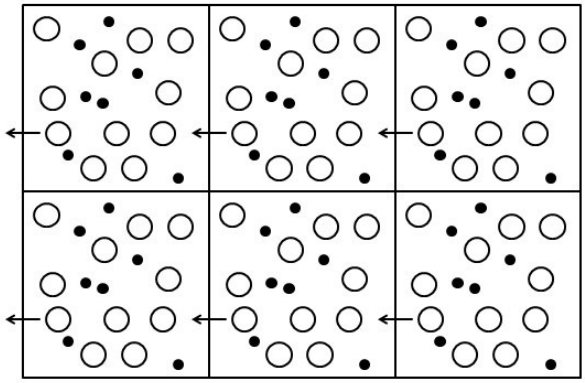

Figure 1.6: Periodic boundary conditions

unit of the PBC is a supercell of the original periodic system. In my research, the unit cell is the same as the repeat unit of the periodic boundary conditions, with some calculations using supercells.

1.4.2 Force Fields

The force field is used to describe the potential energy of a system by defining the molecules' and atoms' interactions, such as bonding, non-bonding, electrostatic and van der Waals interactions. In this project, atom-atom interactions, hydrogen bonding, quadratic bonding and angle interactions, torsion (bond rotation), and non-bonded effects are modelled under the consistent valence forcefield (cvff) [25] as provided by Dr. Hendrik Heinz [26] and the Discover program from Accelrys, Inc. [27] (refer to Chapter 2). It separates the total energy into three parts: non-bonded energy, valence bonding energy and some cross-terms [25].

$$E_{total} = E_{valence} + E_{crossterm} + E_{nonbond}. \tag{1.3}$$

The valence energy can be described as bonding energy, angle and bond torsion,

out of plane interactions and Urey-Bradley atom pairing interactions (angular interactions) [25].

$$E_{valence} = E_{bond} + E_{angle} + E_{torsion} + E_{oop} + E_{UB}. \tag{1.4}$$

Bond energy refers to the energy which is required to break the bonds between pairs of atoms. The relationship of energy E and the distance (separation r) between nuclei is depicted in Figure 1.7 [28]. Mathematically, in our system the bond energy is calculated from the stretch between each bonded pair of atoms assuming a simple harmonic potential (not as complex as that depicted in Figure 1.7):

$$E_{bond} = \sum_{1,2\ pairs\ (bond)} K_b(r_{1,2} - r_0)^2. \tag{1.5}$$

where K_b is an effective "spring constant". Therefore, covalent bond breaking or formation is not well captured by this method. This is appropriate given the types of interactions we wish to model (ionic and hydrogen-bonding).

The stiffness of the bond angle is determined by K_θ:

$$E_{angle} = \sum_{bond\ angles} K_\theta(\theta - \theta_0)^2. \tag{1.6}$$

while K_ϕ determines the rotational barriers for bond torsion or rotation:

$$E_{torsion} = \sum_{1,4\ pairs\ (rotate\ along\ bond)} K_\phi(1 - cos(n\phi)). \tag{1.7}$$

The torsional energy is important to distinguish, for example, the relative energies of staggered and eclipsed conformations of molecules.[28].

The non-bonded energy is a combination of van der Waals (vdW) interactions, Coulombic interactions, and hydrogen bonding interactions.

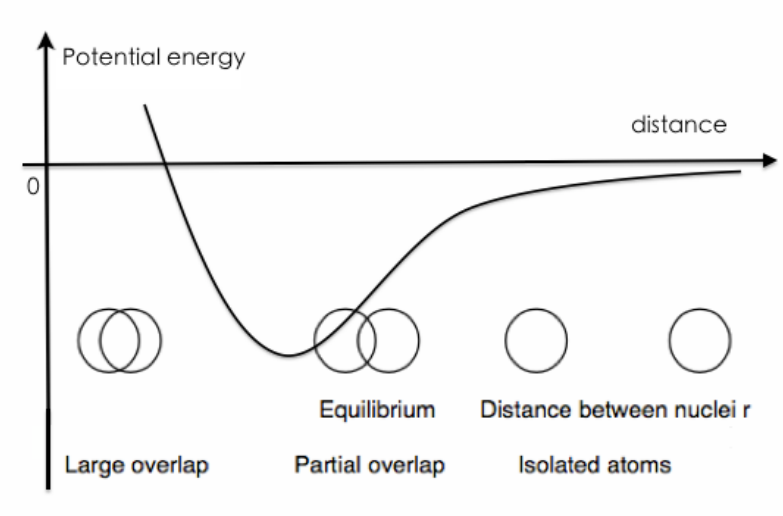

Figure 1.7: Bond energy *vs* distance

$$E_{nonbond} = E_{vdW} + E_{coulomb} + E_{hbond}. \tag{1.8}$$

The van der Waals interaction comes from the repulsive and attractive forces between different molecules (or different parts of the same molecule) which could arise from induced or permanent dipoles. As with covalent bonding and hydrogen bonding, the interaction is strongly repulsive within a short distance, attractive at longer range, and approaches zero at very long distances [29].

The Lennard-Jones potential applied here:

$$E_{vdW} = \sum_{nonbonded\ pairs} (\frac{A}{r^{12}} - \frac{B}{r^6}). \tag{1.9}$$

allows for formation and disruption of intermolecular bonds, following the form of Figure 1.7 albeit on a larger length scale and smaller energy scale. A and B depend on the particles (atom types) involved.

Coulomb's law gives the definition of electrostatic interaction between electrically

charged particles [30]:

$$E_{coulomb} = \sum_{nonbonded\ pairs} \frac{q_a q_b}{D r_{ab}}. \tag{1.10}$$

with q_a and q_b being the charges on the particles, r_{ab} the distance between then, and D is related to the effective dielectric constant of the medium.

1.4.3 Verlet Algorithm

The Verlet algorithm is one of the simplest but best algorithms used for MD simulations due to its accuracy [31]. To derive it, researchers start with a Taylor expansion of the coordinate of a particle about time step Δt. This is the MD time step. The old position with one time step passed and the new position with a new time step ahead can be shown under following equations:

$$r(t + \Delta t) = r(t) + v(t)\Delta t + \frac{f(t)}{2m}\Delta t^2 + \frac{\Delta t^3}{3!}\dddot{r} + O(\Delta t^4). \tag{1.11}$$

$$r(t - \Delta t) = r(t) - v(t)\Delta t + \frac{f(t)}{2m}\Delta t^2 - \frac{\Delta t^3}{3!}\dddot{r} + O(\Delta t^4). \tag{1.12}$$

Adding Equations 1.11 and 1.12 together will produce a new Equation 1.13 and Equation 1.14:

$$r(t + \Delta t) + r(t - \Delta t) = 2r(t) + \frac{f(t)}{m}\Delta t^2 + O(\Delta t^4). \tag{1.13}$$

or

$$r(t + \Delta t) \simeq 2r(t) - r(t - \Delta t) + \frac{f(t)}{m}\Delta t^2. \tag{1.14}$$

The above equations show that the estimation of the new position of a particle

contains an error of order Δt^4, which is very precise. The Verlet algorithm does not use the velocity term to calculate the new position [31], which is good for simulations due to its high accuracy. Meanwhile, Verlet algorithm is very straightforward method for calculating three dimensional motion.

There are other algorithms generated by using a Taylor expansion. Another common algorithm, the Leap Frog algorithm, uses a constant interval spacing for time (Δt_i, Δt_{i+1},...) and centres the velocities at half-time-step positions (Δt_i-$\frac{1}{2}$, Δt_i+$\frac{1}{2}$,...). Higher-order schemes are also used in MD simulations. One of the most popular is called predictor-corrector algorithm [23] .

1.5 Motivation

To reiterate, our motivation is to understand the role of ion and mica surface reconstruction in aligning adsorbate layers. The experimental data relates to large molecules including proteins, which are challenging to model. Here we focus on alignment of water layers, which experimentally may in fact mediate the mica-protein interactions, so that we can figure out whether ions and water can bridge the mica structure (nanoscale) to the protein fibrils (micro-scale).

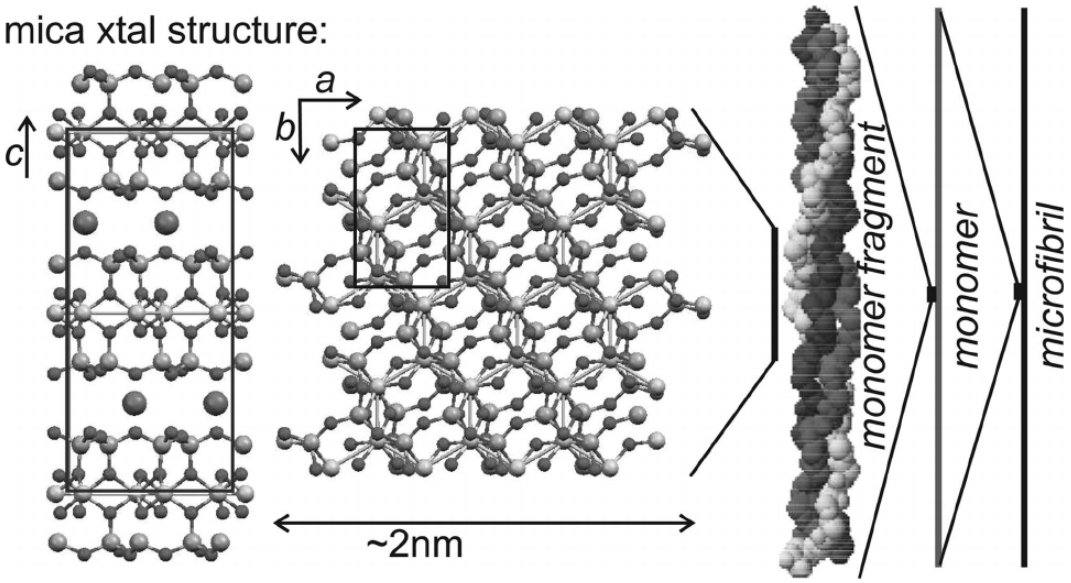

Figure 1.8: Relation between the length scales of the mica crystal structure and protein fibrils [4].

Chapter 2

Software Package & Simulation Methodology

Computational chemistry uses various software packages for molecular modelling and for visualizing output. In order to finally decide which tools to use, researchers should have a good understanding of the advantages and disadvantages of the software.

Computational resources were provided by ACEnet, and Compute Canada. ACEnet, short for the Atlantic Computational Excellence Network, is a network provided by a combination of Atlantic Canadian Universities, who supply high performance computing resources for Atlantic researchers to use. ACEnet is a very powerful network bonded with Compute Canada. It contains many software packages and tools that researchers can request and have free access to use. It is faster than personal computers and has many clusters; different clusters have specific software and tools provided to research groups and industries for computing and visualization.

Figure 2.1: Discovery Studio Visualizer: Molecular modelling tool

2.1 Software Package

LAMMPS [32] is an open-source molecular dynamics software package scripted using C++ [32]. It runs on a single processor or in parallel. It does not provide data visualization (including plotting) tools. LAMMPS can calculate both small systems and very large molecular models under classic Newton's equations of motion [32], which means LAMMPS can generate the system of interest and its motion as a function of time, and the system's forces and energy will be taken into account. Force fields are not provided within the LAMMPS package and must be called from an external source.

Discovery Studio Visualizer [33], also called DS visualizer or DSV, is a free and powerful molecular modelling tool. The DSV software package is designed by Accelrys [34]. DSV can view and edit molecules, display surfaces, and assign solvent for the calculation, which makes it very powerful to use(Figure 2.1) [33].

2.2 Methodology

2.2.1 Generating the LAMMPS Geometry Input Data File

The original geometry for the mica crystal structure was obtained from Dr. Hendrik Heinz [35]. There are two types of geometry files with the file extensions ".car" and ".mdf". The ".car" file contains the information of atoms, atom formal charges, atom

Atom type	Element	Comment
Na	Na	Sodium ion
na+	Na	Sodium ion in phyllosilicates
k+	K	Potassium ion in phyllosilicates
koh	K	Potassium ion in water
na+	Na	Sodium ion in phyllosilicates
h	H	Hydrogen bonded to C
ho	H	Hydrogen bonded to O
h*	H	Hydrogen in water molecule
hspc	H	Hydrogen in SPC water molecule
ay	Al	Aluminum in phyllosilicates, octahedral

Table 2.1: Atom types in ".car" and ".mdf" files with the cvff force field.

types and atoms' x, y and z coordinates. The ".mdf" files consist of atom element, atom types, charges, and connections (bonding information) [1].

The atom types used in these calculations are defined in Table 2.1). The definition of atom types is very important in molecular dynamics calculations, since these calculations forgo a quantum chemical description of the atoms. Atoms of the same element but in diverse environments (bonded to different atoms, in varying solutions, etc) have different atom types. These atom types are associated with those defined in the assigned forcefield.

Because LAMMPS does not provide tools to build input structures, DSV is used for adding atoms (in my project: K^+ and Na^+ ions) and molecules (in my project: H_2O). Simple atoms can be added manually. In order to compare ion effect (by replacing K^+ with Na^+ ions), atoms were put into the structure file at exactly the same positions. A C++ script was used in this case to substitute atoms and add in waters. DSV was used to confirm the structure files are correct. For example, the ".car" file was edited first using C++ scripts, then the new file was viewed by DSV. Once the ".car" file was changed, the corresponding ".mdf" file could also be modified

[1]The file formats are shown in Appendix A.

by changing the atom elements, atom types and formal charges.

The MSI2LMP software package is used for generating LAMMPS geometry input data files (lammps05 files). MSI2LMP is provided in the LAMMPS software distribution and can calculate atom partial charges [2] through ".car" and ".mdf" files' along with the attached force field parameters (from the force field files). In my research, the consistent-valence - phyllosilicates forcefield (cvff_phyllosilicates [35]) is used.

2.2.2 LAMMPS Input Script & Simulation Set Up

The LAMMPS input script constructs the simulation set up, which is built based on the science of the calculations and the performance of the LAMMPS software package. For all simulation models, PBC are applied in three dimensional space, maintaining the same number of atoms during the calculations.

The Coulombic interaction has an isotropic 2.5 Å cutoff.[3] A 0.001 ps (10^{-12} s) time step is used and is considered the standard vibration frequency of the covalent bonds in mica [36]. The "neighbor" "bin" commands were used to store atom pairs in memory with a skin distance of 1.2 Å. This command stores pairwise neighbour lists for all atom pairs within a neighbour cutoff distance equal to the their force cutoff plus the skin distance. The "replicate" command is used to determine whether a unit cell or supercell should be calculated.

I used NPT (isothermal) conditions for my calculations, with Nose-Hoover time integration. [37]. The Nose-Hoover equation updates the position and velocity for atoms in the simulation box for each time step. The system energy is minimized by using LAMMPS "box/relax" feature. The box/relax feature allows the minimization to occur at a user specified temperature which in my case was 293.15 K. As the

[2] These are also called net atomic charges, non-integer charge values in elementary charge units.

[3] This is done using the command "pair_style coul/cut 2.5" and "kspace = ewald/n", where the cutoff is the real space calculation and it is slightly smaller than half of my box size in "a" direction.

pressure in my calculation is fixed to 1 atm, the volume varies during simulations until it reaches an equilibrium state.

During the calculation at selected time steps, velocity and atom positions were generated by using the "dump" command. AtomEye (atomistic configuration viewer) [38] and Avogadro [39] visualization software packages were used for checking output files.

2.2.3 Data Analysis: Pair Correlation Function

To study the organization or reorganization of adsorbate layers (water, in our case), we calculated the pair correlation function $g(r)$ for the oxygen atoms in water for a given layer. Because we were only interested in the surface reconstructions, a two-dimensional $g(r)$ is calculated.

The pair correlation function is a way to express the probability of finding a pair of particles at distance r. The function is essentially a histogram of inter-atomic separations. A histogram represents the distribution of data by separating all data into non-overlapping bins [40]. In my research, water's pair correlation function is calculated so that the water patterns can be checked: to see which distances between water oxygens has the best probability (highest occurrence).

In two dimensions, the pair correlation function $g(r)$ is defined as:

$$g(r) = \frac{1}{N}\frac{1}{2\pi r}\frac{A}{N}\sum_{i=1}^{N}\sum_{j\neq i}^{N}\delta(r - r_{ij}). \tag{2.1}$$

where A is the total area, N is the total number of particles, and r_{ij} is the distance between atoms i and j.

Histograms are often used for density estimation: estimating the probability density function of the underlying variable [40]. Soper et al used the spatial density func-

tion to study low and high density water [41]. Water molecules interacted by hydrogen bonds. Low density water represents a tetrahedral arrangement; this formation gives orientation which affects many chemical, physical and biological properties. In contrast, high density water forms non-tetrahedral angles with oxygens, which involves breaking and reforming many hydrogen bonds. Soper et al put a water molecule in the centre, and by expanding and laying more waters around the central water, empirical potential structure refinement simulations were carried out, and the water density is plotted using a histogram [41] shown in Figure 2.2.

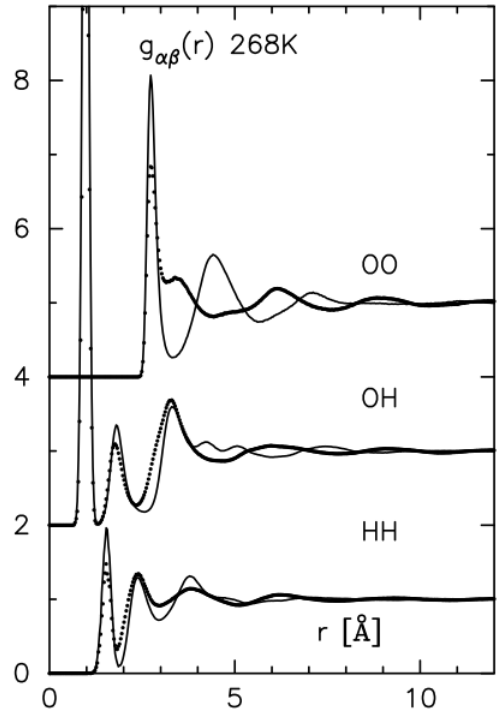

Figure 2.2: Pair correlation functions $g_{\alpha\beta}(r)$ *vs* r for O-O, O-H, and H-H distances in low (lines) and high (circles) density water [41]. The three plots are offset for clarity.

The peak for a given interval in the histogram shows the probability of the data. The higher peak indicates a larger probability of having water separated by that distance. For example, in Figure 2.2, the largest (off-scale) peak in the OH pair

correlation curve shows the most probable O-H bond length. The next peak shows the closest inter-molecular hydrogen bond. The O-O plot in Figure 2.2 shows regular shells of water molecules which become more compressed (peaks closer together) for high density water. A pair correlation function without any features (peaks) indicates a system which is not ordered or structured.

2.2.3.1 Generating Pair Correlation Functions $g(r)$

During simulations, the "dump" command generates ".xyz" files with all of the atoms' coordinates; I generated these for every 250 steps. I wrote a C++ script to assign the atoms their elements by comparing them with the corresponding initial ".car" geometry files. The pair correlation function scripts then operated on these modified .xyz files.

The pair correlation function is completed by three major steps. First I need to give an element name and z coordinate so that the script can select the atoms from that slice at z (see Figure 2.3). Taking silicon as an example, I would choose a silicon layer (z value = 12 Å), then all the atoms in the silicon layer would be selected and their x, y and z values are stored in memory. Because this project is mainly focused on surface reconstruction, which is a quasi-two-dimensional problem, the pair correlation function is calculated in two dimensions. Then PBC are applied to minimize edge effects. From the above steps, the script can count the total number of atoms N.

Then interatomic distances are calculated, and the smallest and biggest distances are generated. The total area A of the simulation cell is related to the the maximum distance, since this is the diameter of the circular area under consideration (refer to Figure 2.4(a)). Since $A = \pi r^2$, the total area here is: $A = (\frac{maximum\ distance}{2})^2\pi$. The total probability of atoms per area is the total number of atoms N divided by area A.

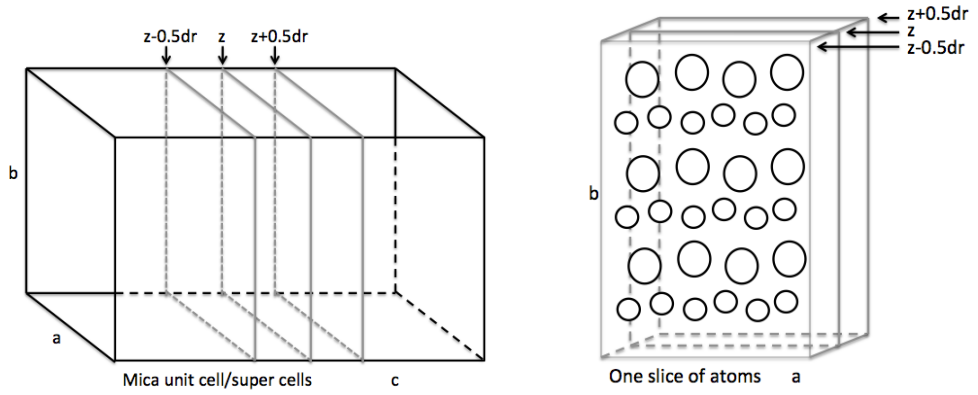

(a) (b)

Figure 2.3: Pair correlation function $g(r)$ scripting steps:(a) Choose the layer (b) Store selected atoms coordination numbers

In the final step, the script counts the instances of distances falling within each bin centered at r with width δr. For each bin (i), the r in Equation 2.1 is the "middle" value of each bin (refer to Figure 2.4(b)). The counts are then normalized by the Equation 2.1 to get a sense of selected atom density in each area.

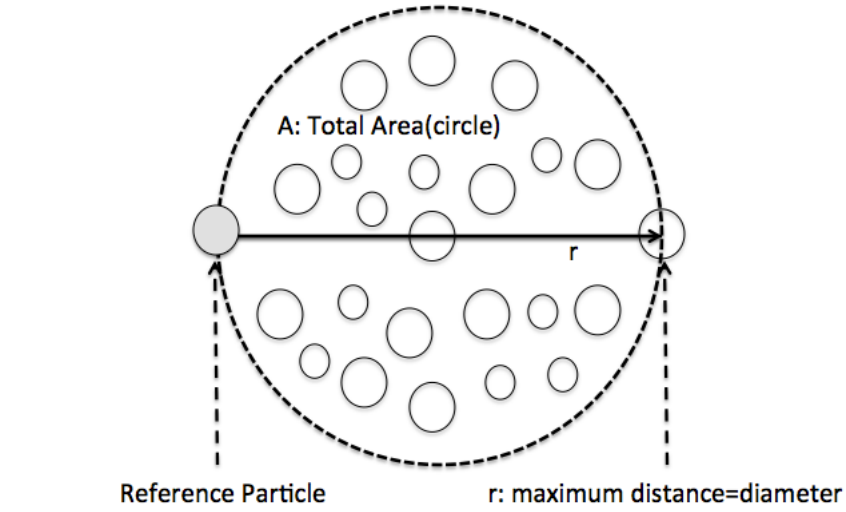

(a)

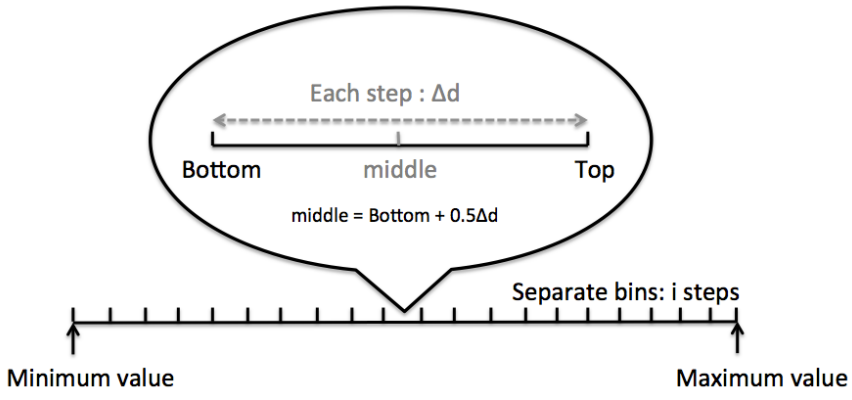

(b)

Figure 2.4: Pair correlation functions $g(r)$: (a) Calculate total area A (b) Looping each bin i, assign each r the "middle" value

Chapter 3

Muscovite Mica: Bulk and Slab Calculations

By experimental methods, previous researchers used muscovite as substrate for imaging protein samples, and found that with mica's rich surface, the sample structure can be affected [4]. Collagen suspensions were deposited on mica surface. Through AFM imaging, collagen showed alignment on the mica surface, and this alignment was ion-dependent [4, 42]. In order to understand the reasons behind this phenomenon, computer simulations are used.

For computer simulations, plain mica was generated under periodic boundary conditions based on the structure from X-ray diffraction data [26]. After the system reached equilibrium, the following effects were checked: the atom movements at each time step, surface reconstruction, unit cell volume and in between the mica layers, Al and Si atom migrations. I considered three different unit cells for the bulk mica simulations: the original unit cell from the X-ray diffraction data, a $2 \times 2 \times 1$ supercell, and a $4 \times 4 \times 1$ supercell.

In this chapter, in addition to calculations on bulk mica, the effects of ions, and

properties of slabs are also discussed. A gap was added between layers in the unit cell for checking the slab effects, and later the potassium ions were replaced by sodium ions in order to check the ions' influence.

After optimizing the plain mica structure, further effects were checked. For example, the effects of water on surface and sub-surface reconstruction were calculated. By adding one or more layers of water on mica surface or adding more ions into the mica layers, the whole unit cell structure varies. These effects are discussed in the next chapter.

3.1 Bulk Mica System

The original mica geometry ".car" and ".mdf" files were provided by Dr. Hendrik Heinz, associate professor at The University of Akron. I redefined the mica structure layers for consistency with later slab calculations, when I would expose the experimentally relevant oxygen- or ion-terminated layer while maintaining periodic boundary conditions.

From the original mica structure file (Figure 3.1 (a)) [26] I transferred the atoms on the right hand side to the left as shown in Figure 3.1 (b), subtracting from the right hand atom's z coordinates the c axis length of the unit cell (19.9453 Å). The initial a and b axis lengths were also set to those provided by the crystal structure data.

3.1.1 Bulk Mica

The final structure for bulk mica after the system reaches equilibrium is quite similar to the starting geometry, indicating that the force field used is reasonable. This bulk mica structure was used as the starting geometry for later calculations, and the

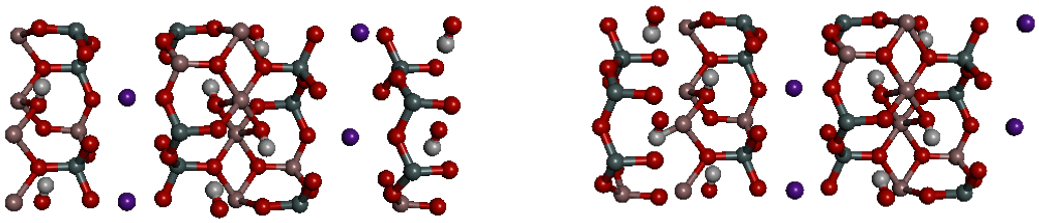

(a) (b)

Figure 3.1: (a) Original mica unit cell structure (b) Modified mica unit cell structure

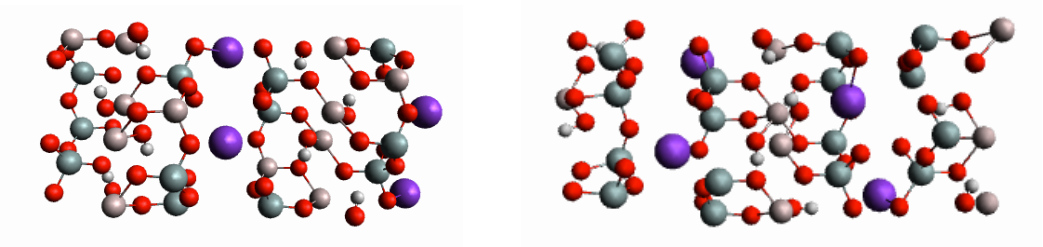

(a) (b)

Figure 3.2: Bulk mica calculation: (a) Original input structure (b) Final output structure

structure is shown in Figure 3.1 (b). The horizontal shift between panels (a) and (b) of Figure 3.1 is merely a result of the periodic boundary conditions. The structure of the layers is maintained after the system relaxes.

The bulk mica structure was considered optimized after convergence. Due to using NPT conditions, the volume of the unit cell could change. This volume was used for the convergence criterion. By the end of the run the volume increases to 1.8885 $\times 10^{-7}$ Å^3 (2.02 $\times 10^{-8}$%) compared to the original input structure.

In order to compare computational data with experimental results, the surface oxygen patterns were checked. The input surface oxygen geometry is shown in Figure 3.3. I calculated the atom positions by averaging over equilibrium geometries. (I averaged 80 snapshots taken every 250 steps, covering overall 20000 steps.) The resultant plots of the surface oxygens use periodic boundary conditions to show the

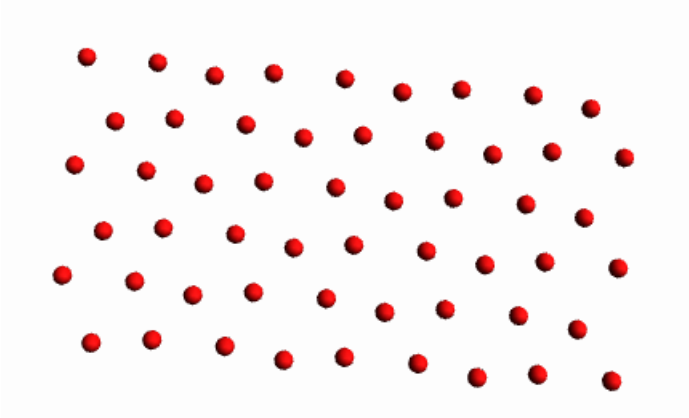

Figure 3.3: Input surface oxygens' geometry

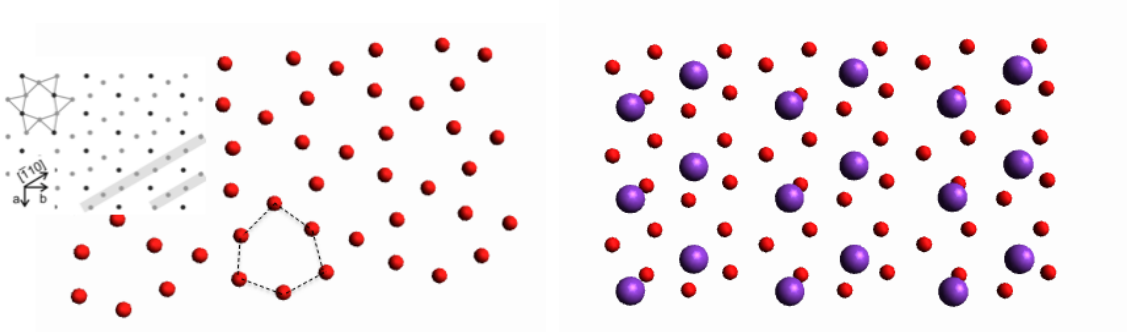

(a) (b)

Figure 3.4: (a) Surface oxygens (red) from the average structure after convergence for the bulk mica system. The inset shows the schematic of the proposed mica (001) reconstructed surface [4]. (b) Surface oxygens (red) with K^+ ions (purple) based on the average structure after convergence of the bulk mica system.

larger area surrounding the unit cell. The average structure after convergence shows a reconstruction of the O layer which is quite similar to that proposed from earlier experimental results [4, 10].

Figure 3.4 (a) shows the average O positions after convergence, with an inset[4] showing the previously proposed surface reconstruction. Therefore our results confirm the surface reconstruction observed by X-ray diffraction [10] and also invoked to explain adsorbate alignment by AFM [4].

3.1.2 Supercell Effects

To allow for longer-range order to evolve if possible, I also studied systems with larger unit cells (supercells). The system with a $2\times2\times1$ unit cell contained the same layered structure but with a unit cell area four times larger in the (001) plane. Similarly, the $4 \times 4 \times 1$ system presented a (001) plane with an area sixteen times larger per unit cell.

Lammps [32] provides a "replicate" command for running super cell systems, wherein the package automatically enlarges the unit cell to super cells and run the calculation with the same input data file as for the original (smaller) unit cell. This method turns out to give disordered structure after the calculation, as shown in Figure 3.5, with, for example, the cations clustering together. The layers of the structure are also completely disrupted. I also manually made a larger unit cell by putting small original unit cells together. For example, in order to study the $2 \times 2 \times 1$ supercell, I used four original unit cells. The results look very similar to those from the runs using the "replicate" command.

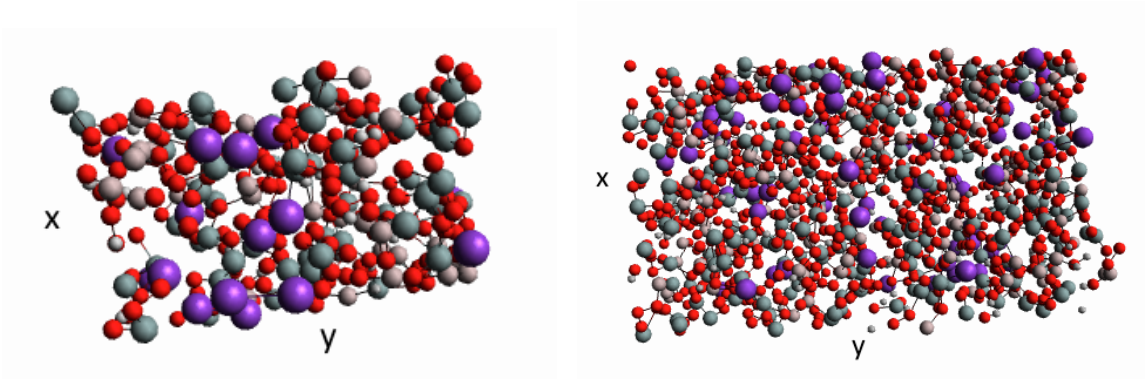

(a) (b)

Figure 3.5: Snapshot of the top view ((001) plane) of bulk mica after convergence for the (a) 2x2x1 supercell and (b) 4x4x1 supercell.

For both the $2\times2\times1$ and $4\times4\times1$ super cell systems, the volume change from the

original structure to the converged structure is quite small, as summarized in Table 3.1. From figures we can hardly see the mica layered features, therefore, the layered structure (and hence the organization between layers) is lost.

The disordered supercell structure might be caused by using a small Coulomb cut-off distance (2.5 Å), thus not properly treating the mid-range and longer Coulomb interactions. (This also applies to the calculations in subsequent sections, where some atoms are fixed.) Longer Coulomb cut-offs can lead to problems in layered systems, particularly charged systems. Mica is a negatively charged system from the oxygen-terminated surface in my calculation: this substantial net charge effect can lead to unstable results. Ordinary approaches to the coulomb interactions, without considering the longer-range impacts in a periodic system, cannot fully address the polarizability and net charge of the system. Rozzi et al talk about how to choose an exact coulomb cutoff for layered systems, particularly charged systems [43]. While Rozzi's work refers to quantum mechanical calculations, the issues also impact classical calculations.

Coulomb interactions are important even for classical systems [44]. Long-range interactions need to be considered especially for charged systems. Fukuda et al compare various methods to include charge effects. The moving boundary reaction field approach treats the solvent as a dielectric continuum when it is outside the cutoff range. This method sets the unit cell centre point as the starting simulation point and replicates the unit cell periodically[45]. The Ewald method I used computes long-range interaction energies of periodic systems in reciprocal space. The cutoff which determines where long-range interactions begin can induce artificial effects.

Cell	Volume Difference	%
$1 \times 1 \times 1$	1.89×10^{-7} Å^3	2.02×10^{-8}%
$2 \times 2 \times 1$	1.09×10^{-4} Å^3	2.92×10^{-6}%
$4 \times 4 \times 1$	6.49×10^{-4} Å^3	4.34×10^{-6}%

Table 3.1: Bulk mica: Volume changes during optimization for unit/super cells

3.1.3 Fixing core atoms

To attempt to maintain the layered structure for the supercells, we decided to fix some atom groups and recalculate the systems of interest. Below are the three positions we chose to fix the atoms, and the results were checked afterwards. In order to get a result which would be more suitable to the experimental situation, we allow a few layers near the mica surface area move while fixing the core atom positions.

There are several ways to define "core atoms" and "surface atoms", particularly since our unit cell contains two aluminosilicate layers. These are defined in Figure 3.6 showing the original unit cell; equivalent definitions were used for the supercells. In case 1, within one slab the core and one face of that slab are fixed, allowing the other face and its adjacent slab to move freely. In case 2, only one face of one slab is fixed, allowing the other face and the other slab to move freely. In case 3, an entire slab is fixed, allowing the atoms in the other slab to move freely. In all cases, the cations were never fixed.

3.1.3.1 Bulk Mica: Smaller Unit Cell with Fixed Atoms

Although there was no need to fix atoms in the simulations of the original unit cell, I performed these calculations as a reference point for the corresponding calculations on the supercell systems. All three ways of fixing atoms yield reasonable geometries which do not vary greatly from the freely simulated geometry. As shown in Figure 3.7, the layered structure is mained, although fixing some layers could lead to distortions

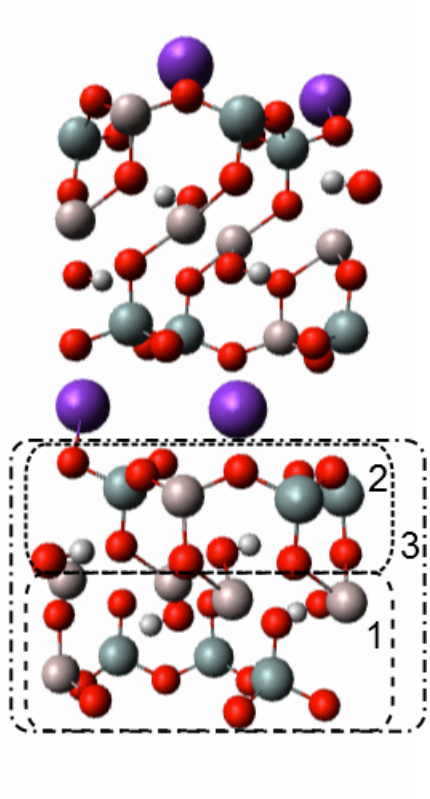

Figure 3.6: Definition of the three sets of atoms/layers being fixed in different calculations.

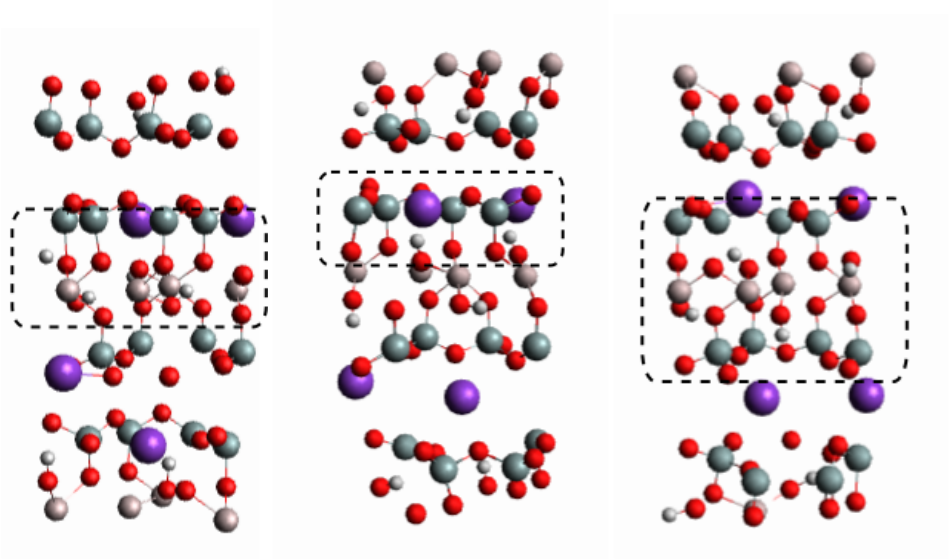

(a) (b) (c)

Figure 3.7: Converged geometry snapshots for the bulk mica unit cell when fixing (a) core and one face (case 1), (b) one face (case 2), and (c) one entire slab (case 3). The dashed box in each case indicates the fixed atoms (not including cations).

in coordination of adjacent atoms. As discussed below, this becomes an issue for the supercells.

In addition to the effect on maintaining the layered structure, fixing atoms could also have effects on lateral organization. Since we are particularly interested in the organization of surface oxygens, I compare those layers here. When fixing an entire slab, the surface oxygens in the adjacent slab (which are not fixed), shown in Figure 3.8a, are very similar to those in the original, freely-simulated structure (Figure 3.4a). However, the arrangement of K^+ ions is quite different when part of the system is pinned (Figure 3.8b) than when the whole system is free (Figure 3.4b). Pinning a part of a slab leads to significant distortions in the average O positions for the free face of that same slab, as see in Figure 3.9.

The reconstruction of the oxygen layer is not just a lateral rearrangement. These changes in position within the layer arise from tilting of silica tetrahedra. Therefore,

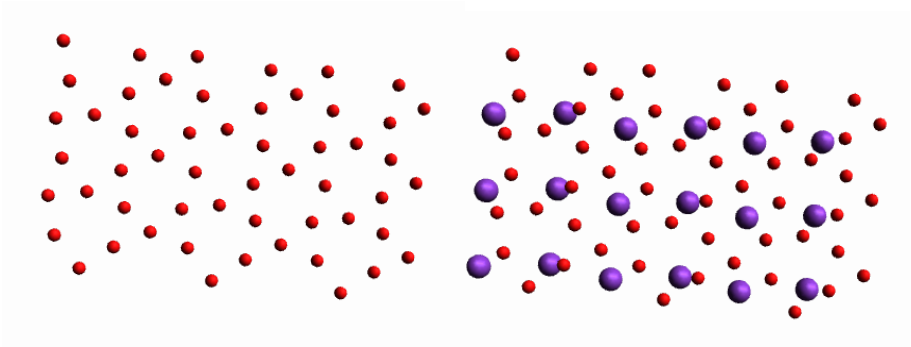

(a) (b)

Figure 3.8: Bulk mica with the original (smaller) unit cell, with one aluminosilicate slab fixed and the other slab plus all cations left free (case 3). (a) Surface oxygens (from the unfixed slab) based on the average structure after convergence. (b) The same surface oxygens with K^+ ions based on the average structure after convergence.

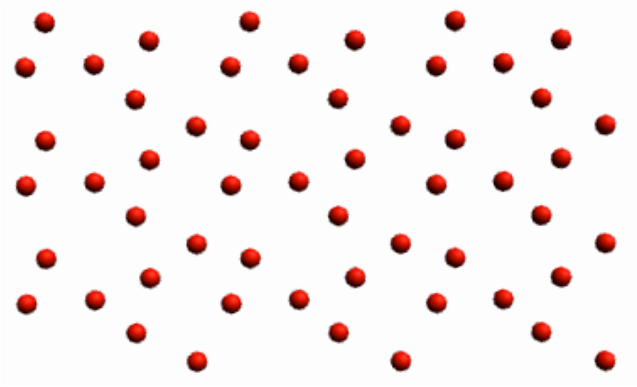

Figure 3.9: Surface oxygens from the average structure after convergence for the bulk mica system with the original (smaller) unit cell, with one silica face of one aluminosilicate slab fixed (case 2).

Fixed atoms	SD (Å)
none fixed	0.034
case 1	0.141
case 2	0.279
case 3	0.114

Table 3.2: Standard deviations (SD) from the average z position within a surface oxygen layer for various systems: no atoms fixed, alumina core and one silica face fixed (case 1), one silica face fixed (case 2), and an entire aluminosilicate slab fixed (case 3).

there is also a puckering of the oxygen layer, which we can quantify from the standard deviation (SD) from the average position in z within an layer defined in the xy plane. The larger the standard deviation, the more tilting there is because some oxygens are lower than the original plane and other are higher. The atoms are initially defined as all having the same z coordinate (all in a perfectly flat layer), therefore the original standard deviation from the average z position would be zero. Table 3.2 lists the standard deviations in z for the oxygen layers for various cases of fixed atoms, with the free calculation as a reference.

In all cases, fixing some atoms led to more puckering in the surface oxygen layers which were not fixed. Although the lateral arrangements are similar between the unfixed system (Figure 3.4a)and the system with one entire slab fixed (case 3, Figure 3.8a), the fixed case shows more puckering as seen by the higher SD in Table 3.2. The case with most puckering, when just the silica face on one slab was fixed (case 2), shows distortions in other layers as well.

Therefore, fixing some atoms does maintain the layered structure, but it can introduce artifacts not observed in the free structure. Bearing that in mind, I applied the fixed scenarios to the supercell systems to see if I could maintain a layered structure and therefore observe some meaningful results on surface reconstruction. However, fixing atoms with supercells did not lead to converged structures. The distortions

observed with the smaller unit cells were magnified with the supercells, compounding the loss of structure observed with the free (unfixed) supercell simulations.

All in all, increasing the mica (001) plane does not show good results, and the supercells turn out to give little useful information for data analysis. Note that our smallest unit cell already contains an area of nearly 50 $Å^2$, with enough atoms to possibly the anisotropic surface reconstructions which we propose are driving the asorbate organization observed experimentally [4]. Therefore, I continue our simulations using the original unit cell to study effects of ion substitutions on the surface reconstruction, seeking a link with the experimental observations of ion-dependent organization [4, 42].

3.2 Ion Effects

3.2.1 Substituting Na^+ for K^+

In order to understand the effect of the ions, K^+ ions were replaced by Na^+ ions, and all previous simulations were recalculated. Experimentally, the collagen suspensions were prepared in either a Na^+ or K^+-containing buffer, and the experimental data motivating this work shows different pattern evolution when using Na^+ than when using K^+ ions. Therefore, we would like to consider the effects of those ions on the structure of mica.

In reality, even in the presence of a Na^+-based buffer there could still be K^+ ions associated with the mica surface, but over time one could imagine an exchange of ions at the interface, with the K^+ ions originally associated with the mica becoming diluted by the Na^+-containing solution. Likewise, there could be ion substitution in the natural mica as well, such that all cations initially associated with the mica are not K^+ [11]. To make a clear comparison I modelled two extremes: one in which all

Cell	Volume Difference	%
$1 \times 1 \times 1$	1.36×10^{-7} Å^3	1.46×10^{-8}%
$2 \times 2 \times 1$	6.87×10^{-5} Å^3	1.84×10^{-6}%
$4 \times 4 \times 1$	4.36×10^{-4} Å^3	2.92×10^{-6}%

Table 3.3: Bulk mica substituted with Na^+: Volume changes during optimization for unit/super cells

cations are K^+ (above) and another in which all cations are Na^+ (here).

By substituting the K^+ ions with Na^+ ions in ".mdf" and ".car" structure files, all the mica structure files were modified. Then all runs were repeated. Although Na^+ is smaller than K^+, the volume of the unit cell did not change a lot. The volume differences from the original input geometry [26] are not large, as summarized in Table 3.3. For example, the original (smallest) unit cell increases in volume by 1.9×10^{-7} Å^3 in the K^+-containing system (Table 3.1) and 1.4×10^{-7} Å^3 in the Na^+-containing system. When moving to the $2 \times 2 \times 1$ supercell, the Na^+-contained system maintains its structure better than did the K^+-contained mica, but the structure is completely lost in the $4 \times 4 \times 1$ supercell system.

The sodium-containing structure also leads to reconstruction of the surface oxygen layer, with strong distortions of the original hexagonal formation yielding more of a triangular shape. This triangular formation in the surface geometry is highlighted in Figure 3.10. (Note that this is a two-dimensional projection of the layer; not all oxygen atoms are in the same plane, and therefore they are not as close as they might appear.) The K^+-containing mica structure also showed distortions of the hexagonal layout of oxygens (Figure 3.4) but the anisotropy was not as pronounced. The change of surface oxygen organizations shows that the ions do effect the mica structure rearrangement.

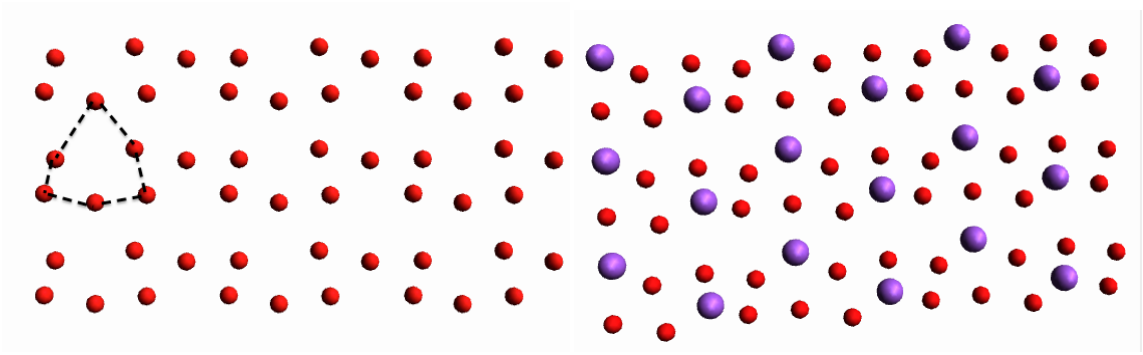

(a) (b)

Figure 3.10: (a) Surface oxygens (red) from the average structure after convergence for the Na^+-substitued bulk mica system. (b) Surface oxygens (red) with Na^+ ions (purple) based on the average structure after convergence of the bulk mica system.

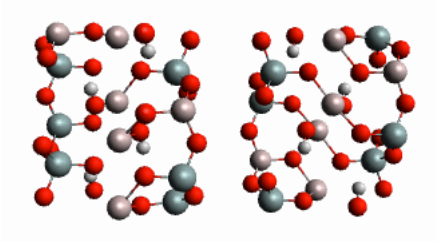

Figure 3.11: Bulk mica unit cell without ions

3.2.2 Removing ions

To further test the effects of ions on the surface structure, and to provide a reference system for some of the water-containing calculations described in the next chapter, although the system is quite unphysical, we also considered mica without any ions. The system is shown in Figure 3.11. This is a highly charged system with a gap of only a few angstroms between the partial negative charges on the oxygens.

Surprisingly there is very little change in the core mica structure. For the no ions system, the converged volume is actually a tiny bit smaller than for the systems containing K^+ or Na^+ ions. The volume changes are summarized in Table 3.4. As with other systems, there is a strong loss of structure in going to larger unit cells

Cell	Volume Difference	%
$1 \times 1 \times 1$	9.84×10^{-8} Å^3	1.05×10^{-8}%
$2 \times 2 \times 1$	1.91×10^{-5} Å^3	5.12×10^{-7}%
$4 \times 4 \times 1$	2.66×10^{-4} Å^3	1.78×10^{-6}%

Table 3.4: Bulk mica without ions: Volume changes during optimization for unit/super cells

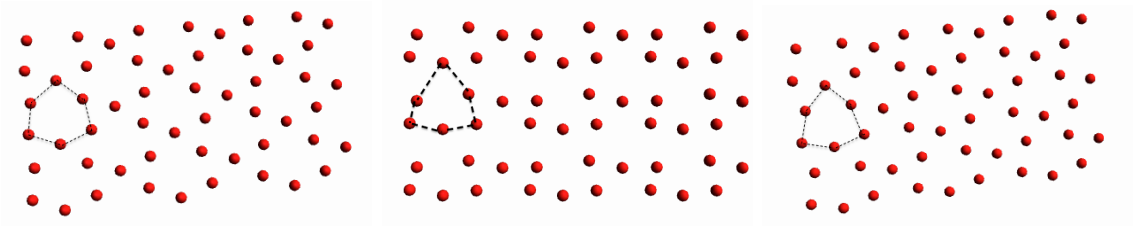

(a) (b) (c)

Figure 3.12: Surface oxygen atoms (red spheres) from the average structure after convergence for the bulk mica system. (a) K^+-containing mica (b) Na^+-containing mica (c) mica without cations.

(supercells).

The arrangement of the surface oxygen layer for the system without ions is very similar to that for the K^+-containing system. Figure 3.12 provides a comparison between the oxygen layers of the three systems considered so far: the bulk K^+-containing mica, the bulk Na^+-containing mica, and the bulk mica without ions. There is a bit more anisotropy (elogantion of the hexagon) in the no ion system, but it is not nearly as distorted as in the Na^+-containing system.

As mentioned in Section 3.1.3.1 above, the lateral rearrangement is accompanied by a puckering of the layer. The puckering in the no-ions system is intermediate to those observed in the K^+- and Na^+-containing systems. This is quantified through the SD in z for the surface oxygen coordinates, as summarized in Table 3.5.

Ions present	SD (Å)
K^+	0.034
Na^+	0.117
no ions	0.109

Table 3.5: Standard deviations (SD) from the average z position within a surface oxygen layer for bulk mica with K^+ ions, with Na^+ ions, or with no ions.

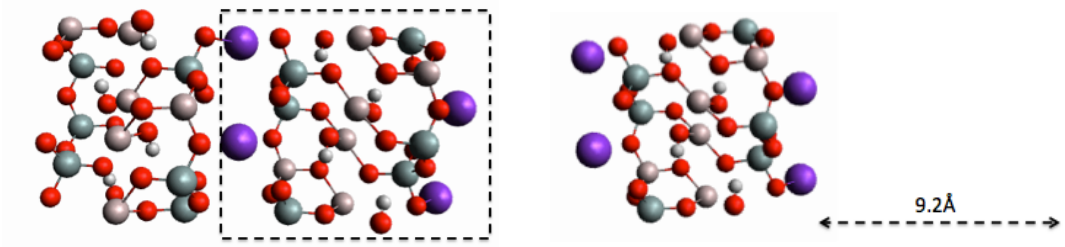

(a) (b)

Figure 3.13: (a) Bulk mica unit cell structure (b) Extracted mica slab: one aluminosilicate layer maintaining K^+ ions on each side

3.3 Slab Systems & Slab Effects

In order to study adsorption on the mica surface, we must expose that surface to the adsorbates. This involves inserting a gap between layers of mica, creating a slab. Before considering adsorbates, we must therefore first consider the effects of creating a slab, comparing its structure to that found in the bulk. In our case, each slab in the mica model is separated by a 9.2 Å empty space, as indicated in the unit cell shown in Figure 3.13b, in comparison to the original structure of the bulk system shown in Figure 3.13a. Calculations on double slabs (gaps between ever second layer) showed similar results.

3.3.1 Mica Slab

The extracted mica structure files were obtained by deleting unwanted atoms from both ".car" and ".mdf" geometry files of the original bulk mica unit cell. The extracted

mica slab consists of K–O–Si–O–Al–O–Si–O–K layers. After simulation, the volume changes are not significant: 1.0335 $\times 10^{-11}$ Å^3, or 1.11 $\times 10^{-13}$% larger compared to the original system.

Inserting a vacuum layer between single aluminosilicate layers does not disrupt the structure of those layers, indicating that this is a reasonable model both structurally and in terms of the force field and other computational parameters. Without the inter-layer interactions, there is an even greater loss of structure within the mica layers upon moving to supercell systems, so these are not discussed further.

3.3.2 Ion Substitution: Mica Slab with Na^+

As with the bulk mica system, K^+ ions were replaced by Na^+ for the slab system. The volume changes are quite small (9.3983 $\times 10^{-12}$ Å^3 or 1.01 $\times 10^{-12}$ % larger) as usual, and smaller than those of the K^+-containing slab perhaps because of the smaller ion size. The pattern formation in the surface oxygen layer follows that of the bulk system.

3.4 Conclusion: the cation does influence the surface reconstruction of the mica

The calculation of the bulk mica system indicates the forcefield that I chose to use is appropriate. Removing ions from original bulk mica does not show a big influence on the geometry, but substituting sodium ions for potassium ions definitely reorganizes the surface reconstruction. Creating a slab system using the same forcefield still gives reasonable results, and changing ions in the slab system show consistent results with regards to the original bulk systems.

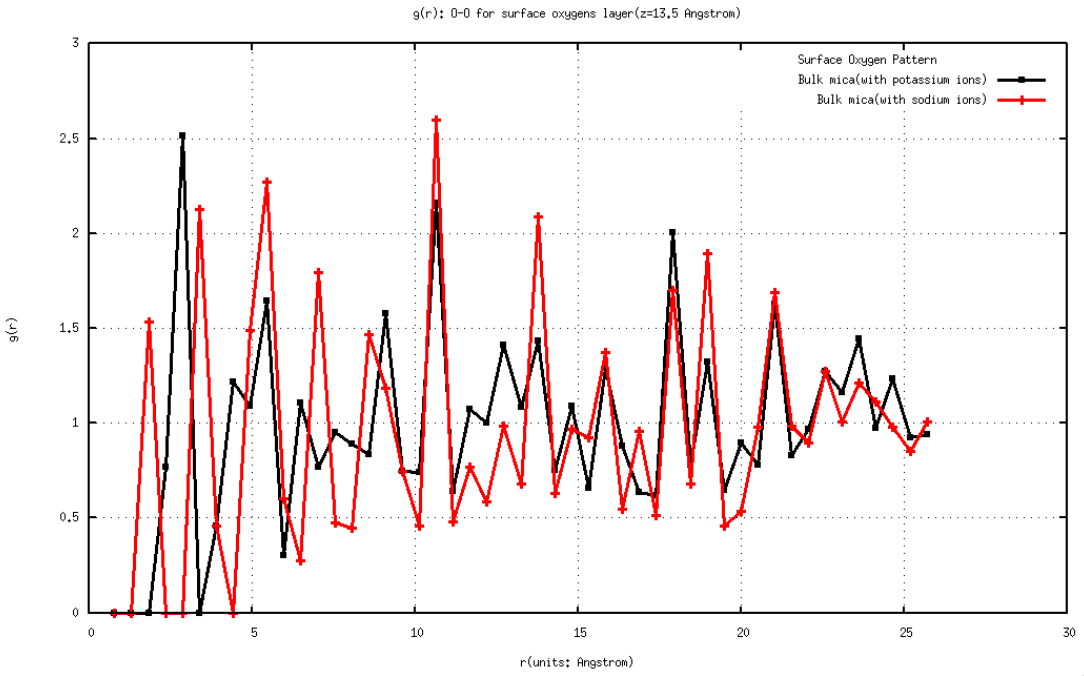

Figure 3.14: O-O pair correlation function ($g(r)$) for the surface oxygen layer, averaged over 80 snapshots taken over 20000 timesteps. The black line is for bulk mica with K^+; the red line is for bulk mica with Na^+.

The changes observed upon changing cation can be further quantified by calculating the two-dimensional pair correlation function ($g(r)$, defined in Section 2.2.3) for the surface oxygen atoms for the different systems. Figure 3.14 compares $g(r)$ plots for the surface oxygen layer for the K^+- and Na^+-containing systems. $g(r)$ for the Na^+-containing system shows a clear doubling of peaks at around 3 Å, while K^+-containing system only shows single peak at region 3Å.

Each peak in the $g(r)$ plot indicates a substantial number of O-O neighbours at that distance r, with the first peak indicating the nearest-neighbour distance. Therefore, the new peak which arises in the Na^+-containing system indicates a new closer contact. In other words, it arises from the anisotropy in the O distribution in that layer. This is illustrated in Figure 3.15. The oxygens forming hexagons in the K^+-containing system are about equidistant, with d1$\sim$d2 (Figure 3.15a). However, in

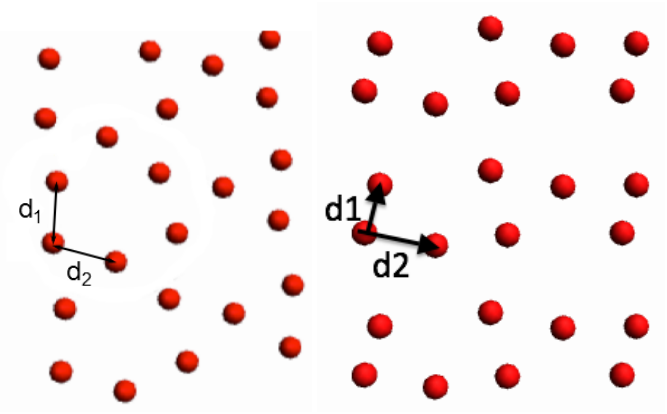

(a) (b)

Figure 3.15: Definitions of nearest- and next-nearest-neighbour distances in the distorted hexagons of the surface oxygens in bulk mica. (a) K^+-containing system (b) Na^+-containing system

System	d1 (Å)	d2 (Å)
Bulk mica with K^+	2.704	2.626
Bulk mica with Na^+	1.366	2.708

Table 3.6: Values of nearest- and next-nearest-neighbour distances between surface oxygens with two different cations.

the Na^+-containing system, one of those distances (as projected in a two-dimensional plane) becomes significantly shorter, such that d1≠d2 (Figure 3.15b). These distances are also listed in Table 3.6. [1]

[1]The oxygen layer is in the range of 1Å in this case, it is not a very deep layer.

Chapter 4

Water Organization on the Mica (100) Surface

In this chapter I present results on the full mica-ions-water system, looking at effects of mica on water, but also at effects of the presence of water on the mica system. These results are for mica slabs, that is to say mica with a gap between individual aluminosilicate layers.

Unless specifically removed, water will be found everywhere in an atmospheric experimental setup even if not in solution. This environmental water can form layers, particularly on hydrophilic surfaces. Therefore, when mica is exposed as a substrate, water is certainly on the top mica layer. After optimizing the mica unit cell alone (shown in the Chapter 3), water was added to the system in order to see whether it would play a role in structural change or not. Surface water and mica layer positions were checked for each time step, in order to know the role waters play in mica reconstruction.

In this project, surface reconstruction is our main interest. Atoms at the surface area encounter interatomic forces from the sides and "below" (defining the "up" di-

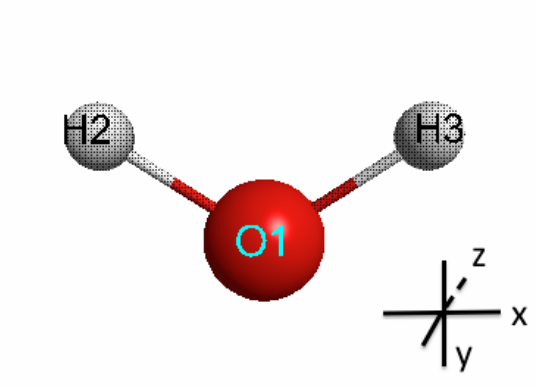

Figure 4.1: Water: oxygen and hydrogens'

Atom Label	x	y	z
O1	0.0000	0.0711	-0.0000
H2	-0.8981	-0.5640	-0.0000
H3	0.8981	0.5640	-0.0000

Table 4.1: Water coordinates (in Å)

rection as the vacuum, gas or solution in contact with the surface). The atoms at the surface alter their arrangement relative to bulk atoms due to this altered force [46].

4.1 Methodology: Building the system

Water was added at the mica surface in the 9.2 Å gap between slabs. This thickness of a water layer is reasonable to observe water structuring, since the experimental evidence indicates that the protein ordering is in the immediate vicinity of the surface [4], and the ordered water layer above mica is thinner than this [47]. I wrote a C++ script for adding waters to the ".car" and ".mdf" files. By running the script, one layer or multiple layers of waters were added into the mica unit cell.

First I built a water molecule to define the relative positions and coordinates of the oxygen and hydrogens (see Figure 4.1 and Table 4.1). Then I placed the oxygen atoms, keeping them at a reasonable distance so that waters are not too crowded from

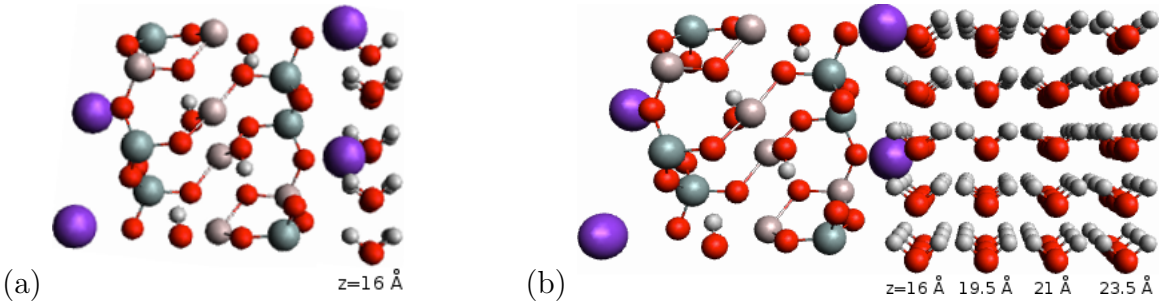

Figure 4.2: Slab systems with water. (a) A single layer of waters was added onto the slab (z=16 Å) (b) Multiple layers of waters were added onto the slab (z=16, 19.5, 21, 23.5 Å)

one and the other or with the surface. Finally, the H atoms were placed relative to their corresponding O. If the oxygen position is (x,y,z), then one hydrogen would be at (x - 0.8981, y - 0.5640, z) and the other hydrogen would be at (x + 0.8981 , y + 0.5640, z).

Figure 4.2 indicates how the mica unit cell would look after adding one (a) or multiple (b) layers of waters. This artificially-structured starting point (square or cubic arrays of water) simply served as a fixed baseline from which to observe water structuring in the presence of mica. Both ".car and .mdf" structure files were changed using the script, and through the MSI2LMP routine the LAMMPS [32] data file was produced for use.

4.2 K^+-terminated Slab Mica Systems

In this research project, detecting whether ions form patterns or specific arrangements on top of the mica layers is the main goal, as this arrangement may be the mechanism for the alignment of proteins on mica which has been observed experimentally[4]. As shown in the previous chapter, my simulations yield different ion arrangements depending on whether K^+ or Na^+ is used. Here I study whether these different arrangements result in different structuring of water adsorbed on or near to the surface.

In all cases, the surface atom geometries are averaged over 80 equilibrium geometries taken every 250 steps, covering overall 20000 steps.

4.2.1 K^+-terminated Mica Slab with One Water Layer

Mica contains K^+ ions between layers, and these ions were maintained to passivate the exposed surfaces in the slab model. A single layer of water was added next to one cation layer. Then the arrangement of water molecules and ions was checked. For this and the other systems calculated in this chapter, even those involving additional cations, the volume changes of the unit cells were very small. These are all collected in one table, Table 4.2.

Model	Volume Difference	%
K^+, one H_2O layer	8.03×10^{-6} Å^3	8.60×10^{-7} %
K^+, multilayer H_2O	4.22×10^{-4} Å^3	4.52×10^{-5} %
K^+, multilayer H_2O + K^+	5.71×10^{-4} Å^3	6.11×10^{-5} %
no ions, one H_2O layer	7.20×10^{-6} Å^3	7.71×10^{-7} %
no ions, multilayer H_2O	4.37×10^{-4} Å^3	4.68×10^{-5} %
Na^+, one H_2O layer	4.30×10^{-6} Å^3	4.61×10^{-7} %
Na^+, multilayer H_2O	4.01×10^{-4} Å^3	4.30×10^{-5} %
Na^+, multilayer H_2O + Na^+	3.20×10^{-4} Å^3	3.43×10^{-5} %

Table 4.2: Volume differences for unit cells of slab systems after simulation.

In comparing surface oxygens of the slab mica system without water to the slab mica system with one water layer, we found that the hexagonal shape is strongly distorted and harder to see after adding the water layer, as seen in Figure 4.3. There are two contributing factors to these changes, which are supported by experimental data. [13] There is likely a direct influence from the water layer oxygens through

hydrogen bonding. Furthermore, the water can impact the influence of potassium ions, and we have seen in the previous chapter that potassium ions are important for generating the tilted reconstructed hexagonal pattern.

We can see the influence of the single water layer on the potassium ions through the standard deviation of the z coordinate (normal to the surface) of the potassium ions. This value increases significantly upon adding water (Table 4.3), indicating that the ion layer is broadening and is therefore not as tightly associated with the mica surface.

Model	Standard deviation in z (Å)
bulk mica	0.795
mica slab	0.658
mica slab, one H_2O layer	2.686
mica slab, multilayer H_2O	2.623
mica slab, multilayer H_2O, with more K^+	2.906

Table 4.3: Standard deviations (in Å) of K^+ z coordinates for various models of potassiated mica after equilibration.

The water layer itself organizes along the direction of the ion stripes, as seen in Figure 4.4a. Figure 4.4b shows the two-dimensional pair correlation function for the oxygens in the water layer in the input structure (black line) and after equilibration (red line). The two peaks at about 3 Å and 6 Å show the nearest-neighbor (within a stripe) and next-nearest-neighbour (adjacent stripe) distances.

4.2.2 K^+-terminated Mica Slab with Multiple Water Layers

More waters were added onto the slab, inserted in the 9.2 Å gap above the mica slab surface. Interestingly, the multiple water layers better maintain the surface oxygen

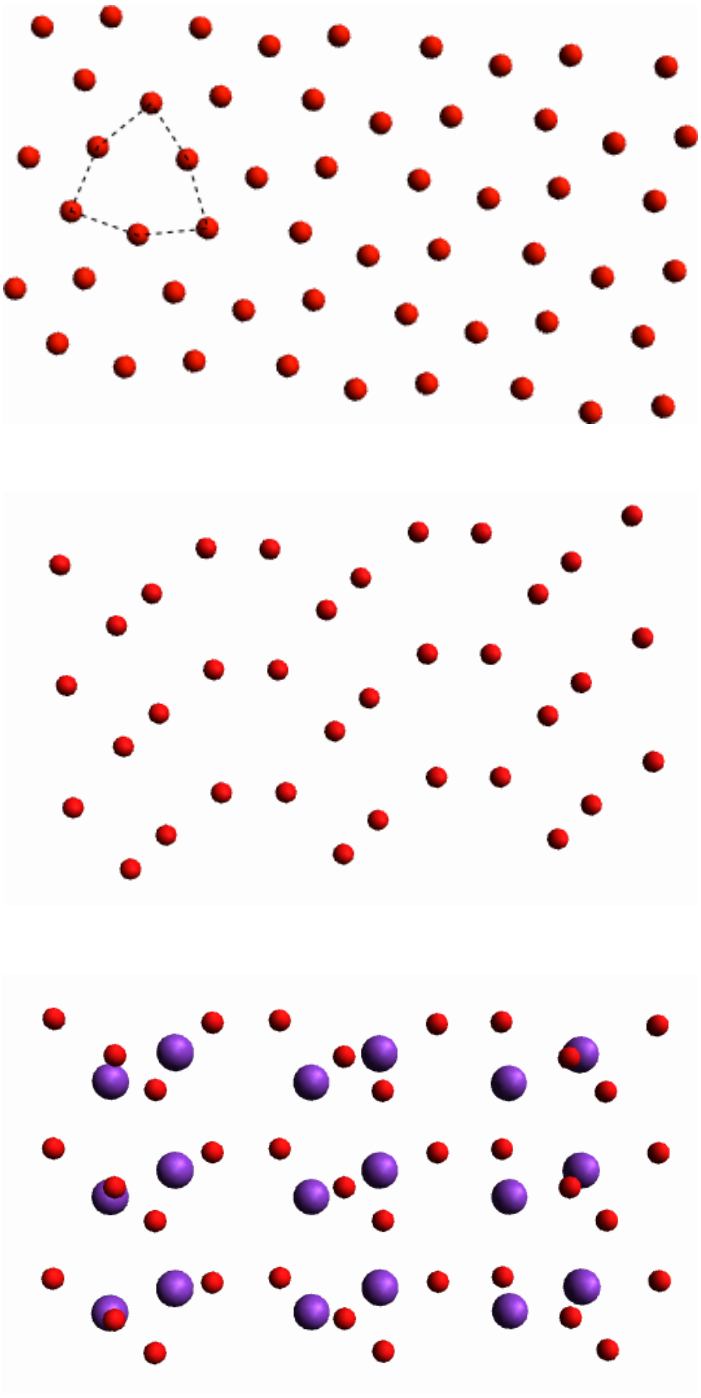

Figure 4.3: Surface oxygen patterns for (a) slab mica and (b) slab mica with one water layer. Panel (c) shows the K^+ ions superimposed on the surface oxygens for the slab mica with one water layer.

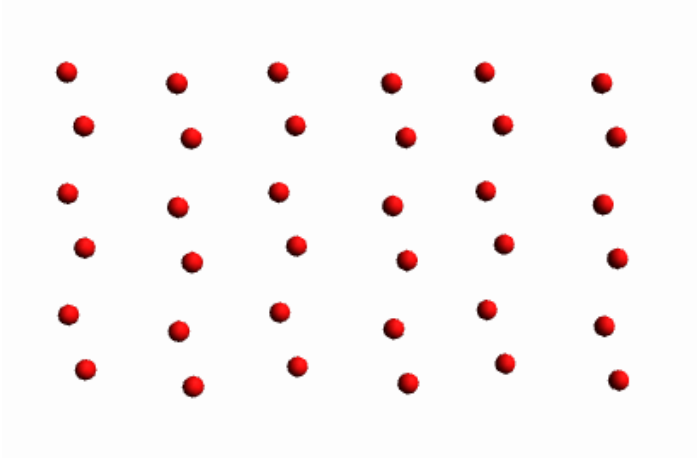

(a)

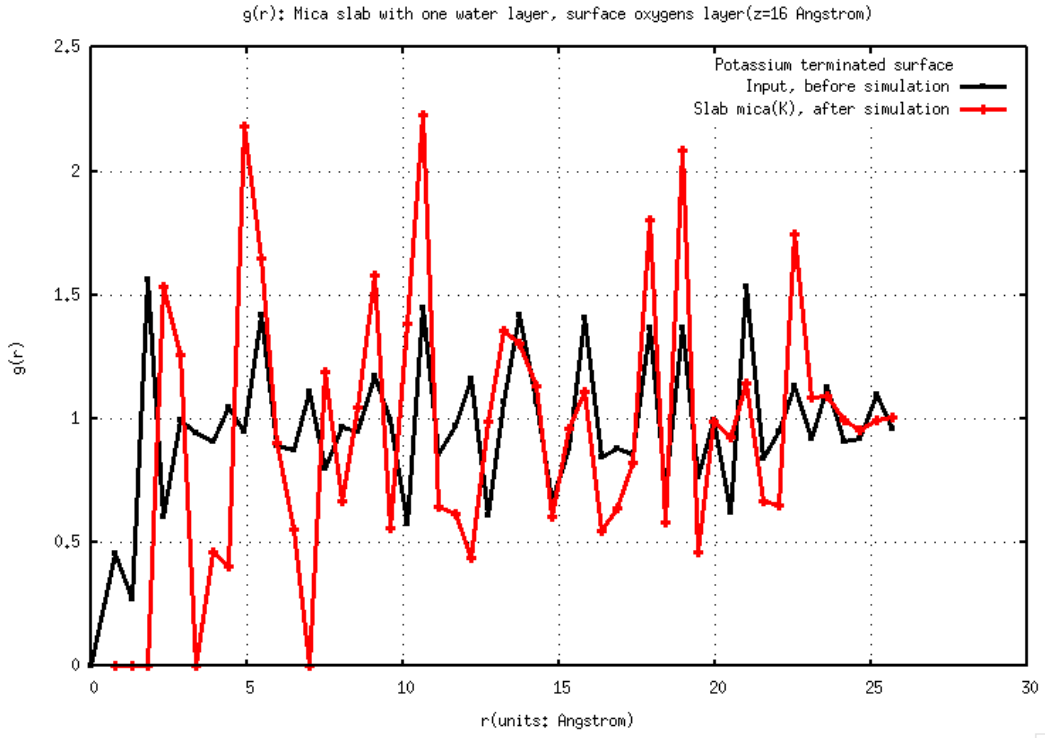

(b)

Figure 4.4: Mica slab with one water layer on a potassium-terminated surface (a) Water oxygen plots (b) Two-dimensional pair correlation functions for water slice in a mica slab with one layer of water. The black line is from the original input structure and the red line is from the equilibrated structure.

reconstruction seen in the slab without water. Figure 4.5a shows the surface oxygens for the mica slab with multiple water layers, highlighting the distorted hexagons. For comparison, the original (input) geometry for the surface oxygens is shown at upper right, with the surface oxygens on the slab without water shown at lower right.

The resulting potassium layer is quite different, though, as seen in Figure 4.5b. In going from no water (Figure 3.4b) to one water layer (Figure 4.3c) to multilayers of water (Figure 4.5b) the potassium ions form more defined rows. In both the single and multilayer water systems, the potassium ions are spread over a larger region normal to the surface (z direction), as quantified in Table 4.3.

Two-dimensional pair correlation functions show the evolution of structure across the different layers of water oxygens. Figure 4.6 shows the two-dimensional pair correlation functions for various layers of water oxygens, with that for the input geometry for comparison. The layers at z = 6 Å and z=19 Å are closest to mica faces, while those at = 8.5 Å and 16.5 Å are in the middle (furthest from mica faces). Because of periodic boundary conditions, the layer which is furthest from one face is closest to the opposite face.

The peak at around 3 Å disappears as we move further from the mica surface, indicating a loss of order in the short-range water-water interactions. The middle water layers are not as influenced by the mica surface or the ions, with water-water (hydrogen-bonding) interactions dominating the structure. The specific effects of the ions in ordering the first layer of water is explored further by removing the cations and by replacing K^+ with Na^+, as described below.

The definition of layers of water is somewhat arbitrary, but it is a useful way of identifying changes in structure as we move away from the surface. Another measure of changes in those layers is to monitor the standard deviation in z for the O atoms in the water molecules. The initial structure has perfect layers, so that the standard

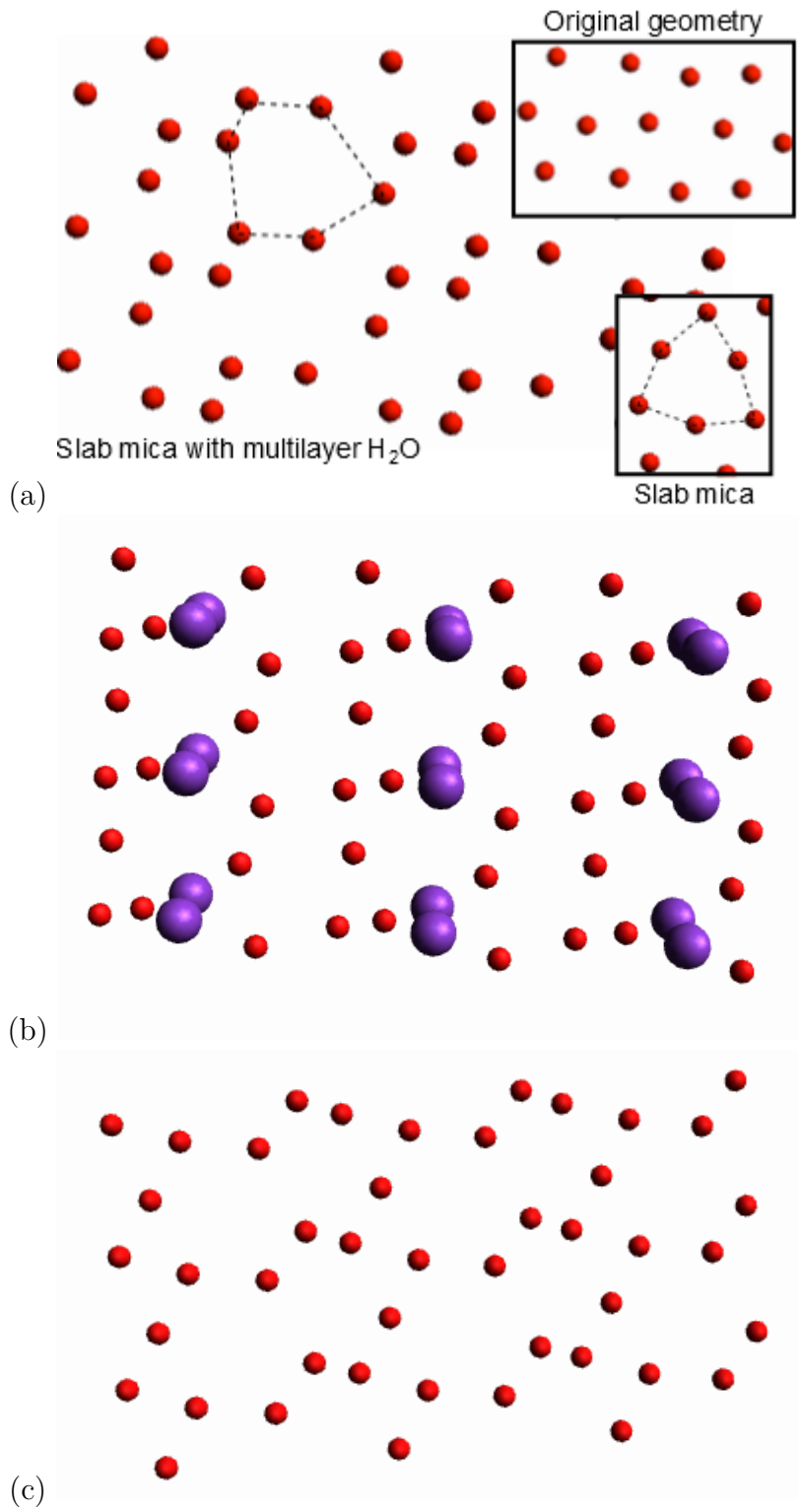

Figure 4.5: Mica slab with multiple water layers. (a) Surface oxygens alone (b) Surface oxygens with ions (c) First slice water oxygens

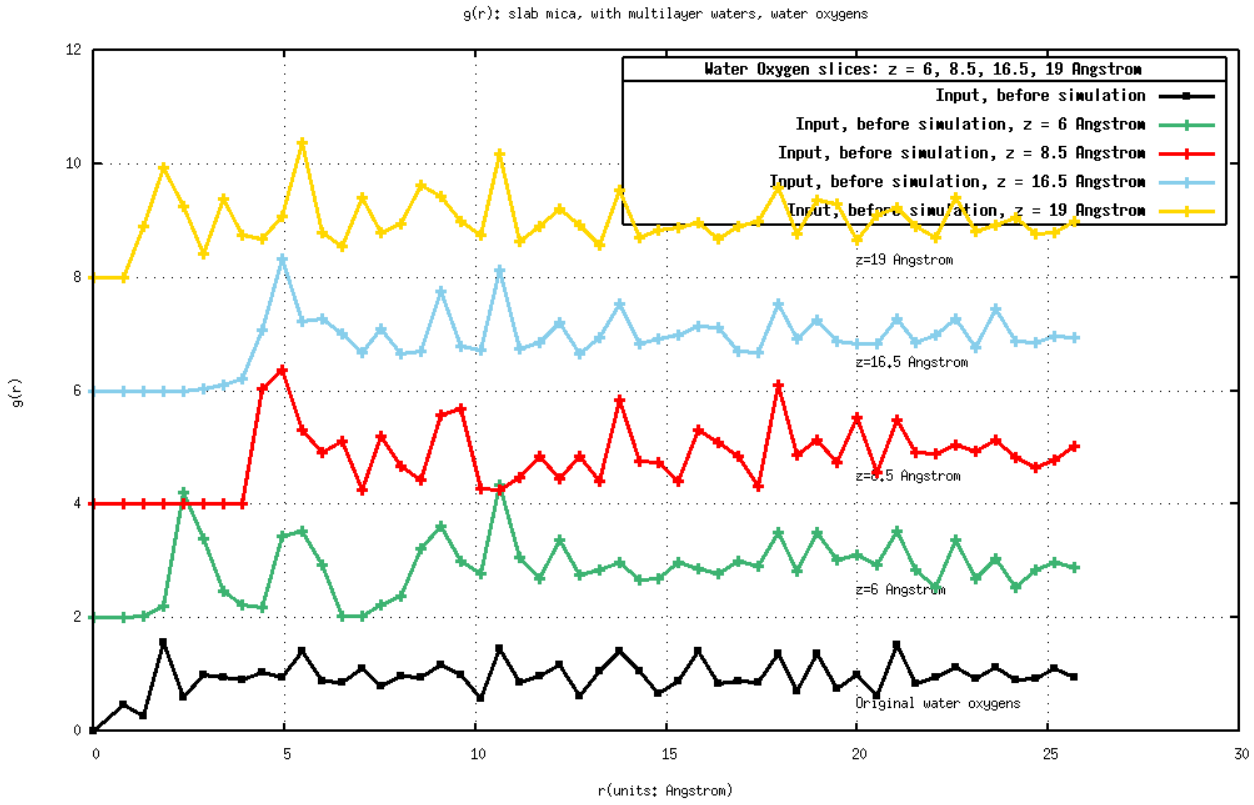

Figure 4.6: Two-dimensional pair correlation functions for water oxygens within different water layers on a mica slab. The black line is from the original input structure (all layers identical). The other plots, offset for clarity, show pair correlation functions at the last step of the simulation for slices at z=6 Å (green), z=8.5 Å (red), z=16.5 Å (blue), and z=19 Å (yellow).

deviation would be 0 Å. In the model with one water layer, the layer "swelled" a bit as it organized, resulting in a standard deviation of 0.21 Å (see Table 4.4). With multiple water layers this grows to 0.68 Å for the first water layer, due to increased interactions with subsequent water layers.

Model	Standard deviation (Å)
K^+, one H_2O layer	0.209
K^+, multilayer H_2O	0.684
K^+, multilayer H_2O + K^+	0.345
no ions, one H_2O layer	0.611
no ions, multilayer H_2O	0.376
Na^+, one H_2O layer	1.569
Na^+, multilayer H_2O	0.459
Na^+, multilayer H_2O + Na^+	0.172

Table 4.4: Standard deviations (in Å) of water oxygen z coordinates for a water layer adjacent to the mica slab.

4.2.3 Additional K^+ Ions within Water Layers on a K^+-terminated Mica Slab

Additional ions were added into the water layers by replacing two waters with two cations in the water layers farthest from the mica. The surface oxygens and the first layer of waters are both restructured (Figure 4.7), with changes in the local coordination environment as seen in the pair correlation functions (Figure 4.8). The pair correlation functions show the nearest-neighbour peak at shorter distance for all water layers, showing ion patterning effects in the middle water layers whose structuring had been dominated by hydrogen-bonding in the plain, multiple water layer model. In

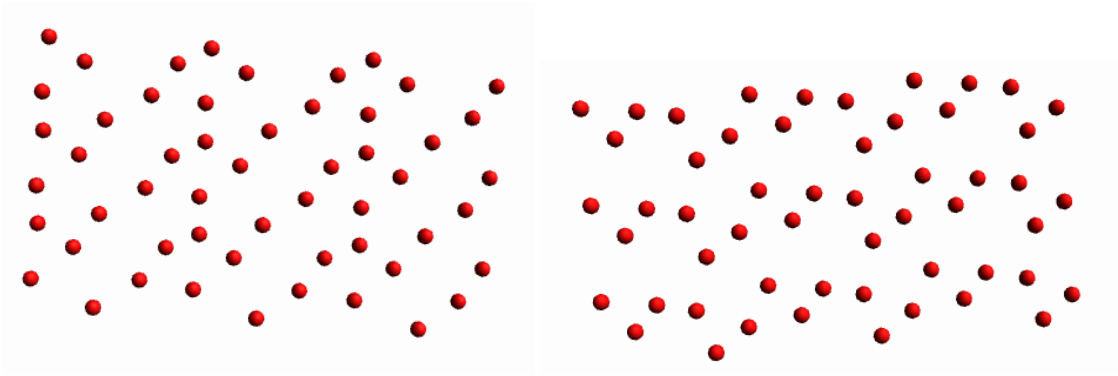

(a) (b)

Figure 4.7: Mica slab with multiple water layers containing potassium ions on a potassium-terminated surface: (a) Surface oxygen (b) First layer water oxygen

other words, the ion effect is dominant compared to hydrogen bonding for the water layers when additional ions are inserted.

Another effect of adding ions to the water layers is a shrinking of the width of the first water layer (0.35 Å) back toward its value in the single-water-layer model (0.21 Å), as seen in Table 4.4. The potassium ions are about equally dispersed in z (normal to the surface) whether additional ions are added to the water or not, as seen in Table 4.3.

4.3 Ion-free Slab Mica Systems

The four K^+ ions, along with their parameters, were deleted from the mica slab ".mdf and .car" structure files. The modified files were then converted into a LAMMPS data file through MSI2LMP for the ion-free simulations. While this system might seem very unphysical, it provides a reference point for comparison with the potassium- and sodium-containing models. Despite the net negative charge of the mica layer, the overall system maintains its integrity as outlined below. However, the water structuring is much weaker without the potassium ions.

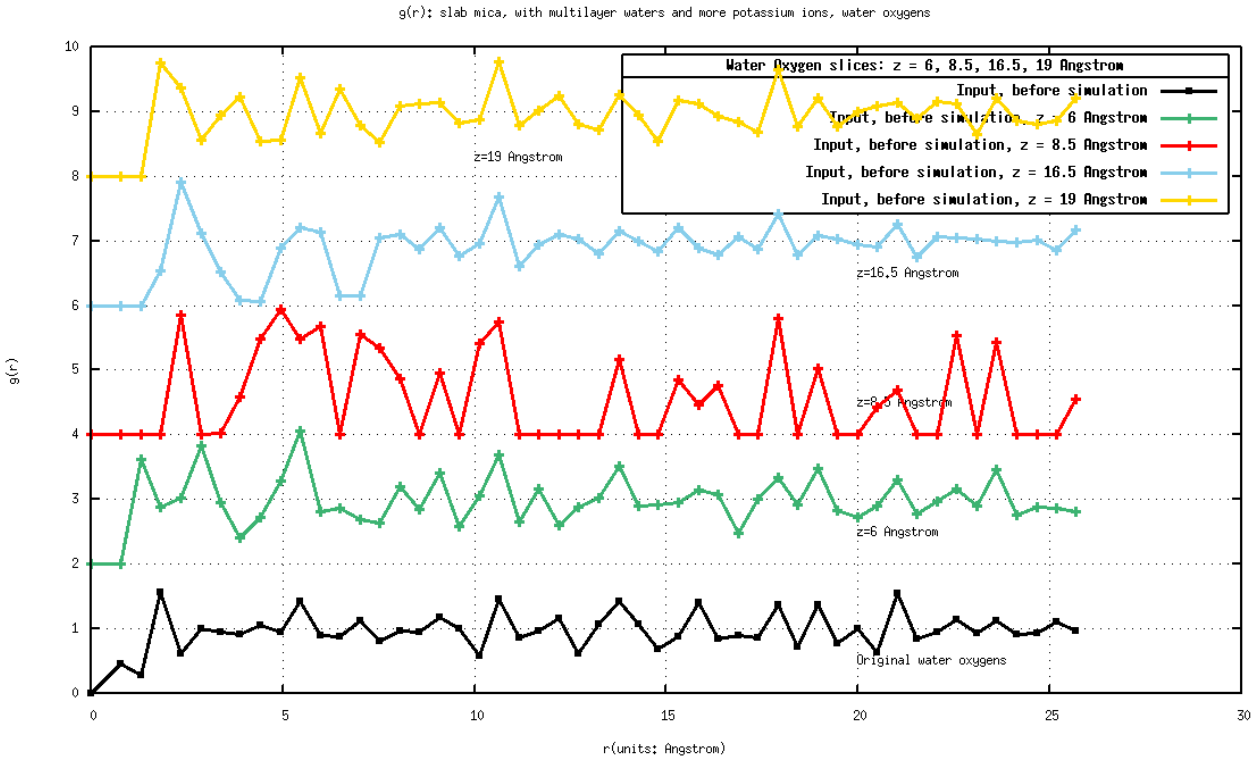

Figure 4.8: Two-dimensional pair correlation functions for water oxygens within different water layers on a potassium-terminated mica slab, where additional potassium ions have bene added to the water. The black line is from the original input structure. The other plots, offset for clarity, show pair correlation functions at the last step of the simulation for slices at z=6 Å (green), z=8.5 Å (red), z=16.5 Å (blue), and z=19 Å (yellow).

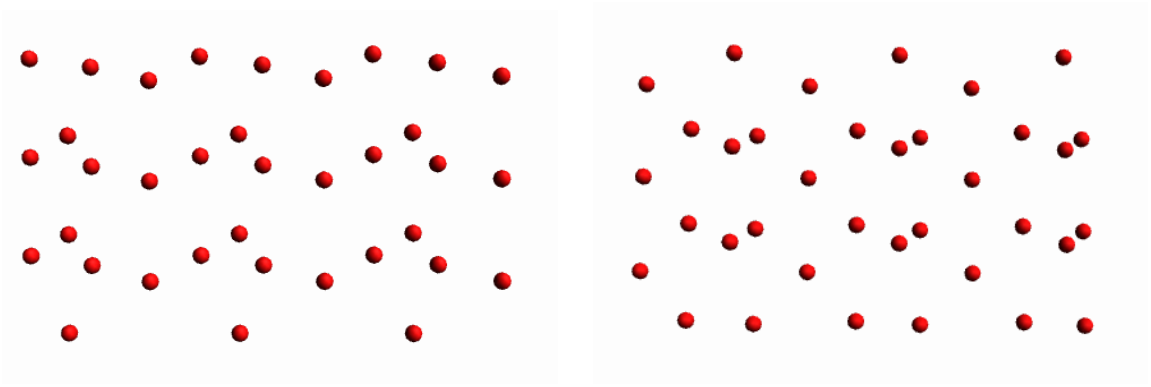

(a) (b)

Figure 4.9: Mica slab (ion-free) with one water layer. (a) Surface oxygens (b) Water oxygens

Average structures for the oxygens at the mica surface and those in the water layer are shown in Figure 4.9. Note that the water layer in the system without ions is now adjacent to a negatively-charged oxygen-terminated surface rather than a positively-charged potassium-terminated surface. Therefore, the surface oxygens and water oxygens showing similar patterns because there are no ions and therefore the main influence comes from hydrogen bonding.

The lack of ions is also seen in the multilayer system, where the pair correlation functions for the various water layers are similar and show similarly weak structure for the most part (Figure 4.10). Because hydrogen bonding is responsible for structuring in all layers, they experience similar arrangements whether adjacent to the mica surface or not. This indicates that the mica structure alone does not greatly influence the structuring of the water, without the intermediate translation of the pattern via the cations.

4.4 Na^+ Ions Contained Slab Mica Systems

Na^+ ions replaced all of the K^+ atoms in the previous simulations, with one or multiple

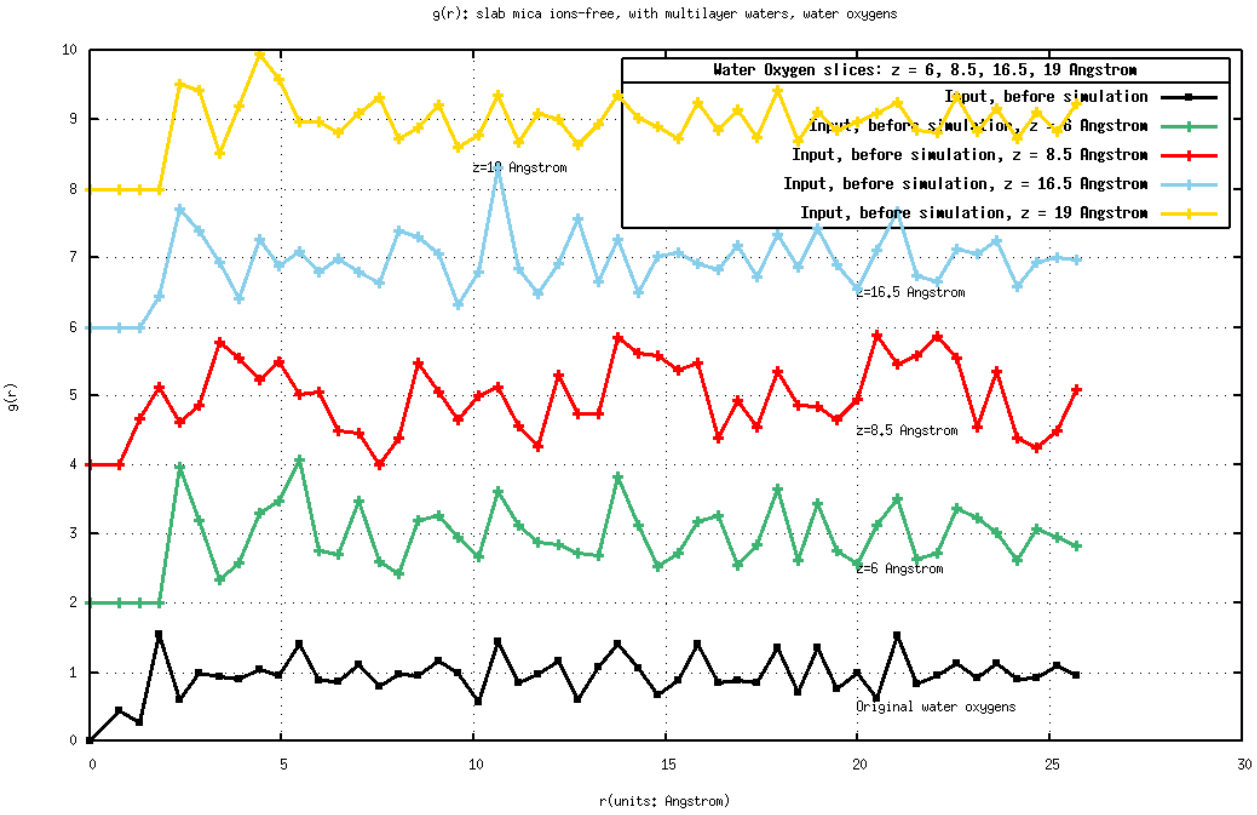

Figure 4.10: Two-dimensional pair correlation functions for water oxygens within different water layers on an ion-free mica slab. The black line is from the original input structure. The other plots, offset for clarity, show pair correlation functions at the last step of the simulation for slices at z=6 Å (green), z=8.5 Å (red), z=16.5 Å (blue), and z=19 Å (yellow).

layers of water added.

4.4.1 Na^+ Ions-terminated Mica Slab with One Water Layer

When Na^+ ions substitute K^+ ions, adding the single layer of water results in a quite different structure for the surface oxygens and the sodiums (Figure 4.11a and b), and therefore also for the water oxygens adjacent to the mica surface (Figure 4.11c). The sodium ions for a much tighter layer, resulting in a smaller standard deviation in z for the sodium ions (Table 4.5) than for the potassium ions (Table 4.3) in the single-water-layer model. The water layer, on the other hand, is much more expanded (see Table 4.4) than in the potassium model.

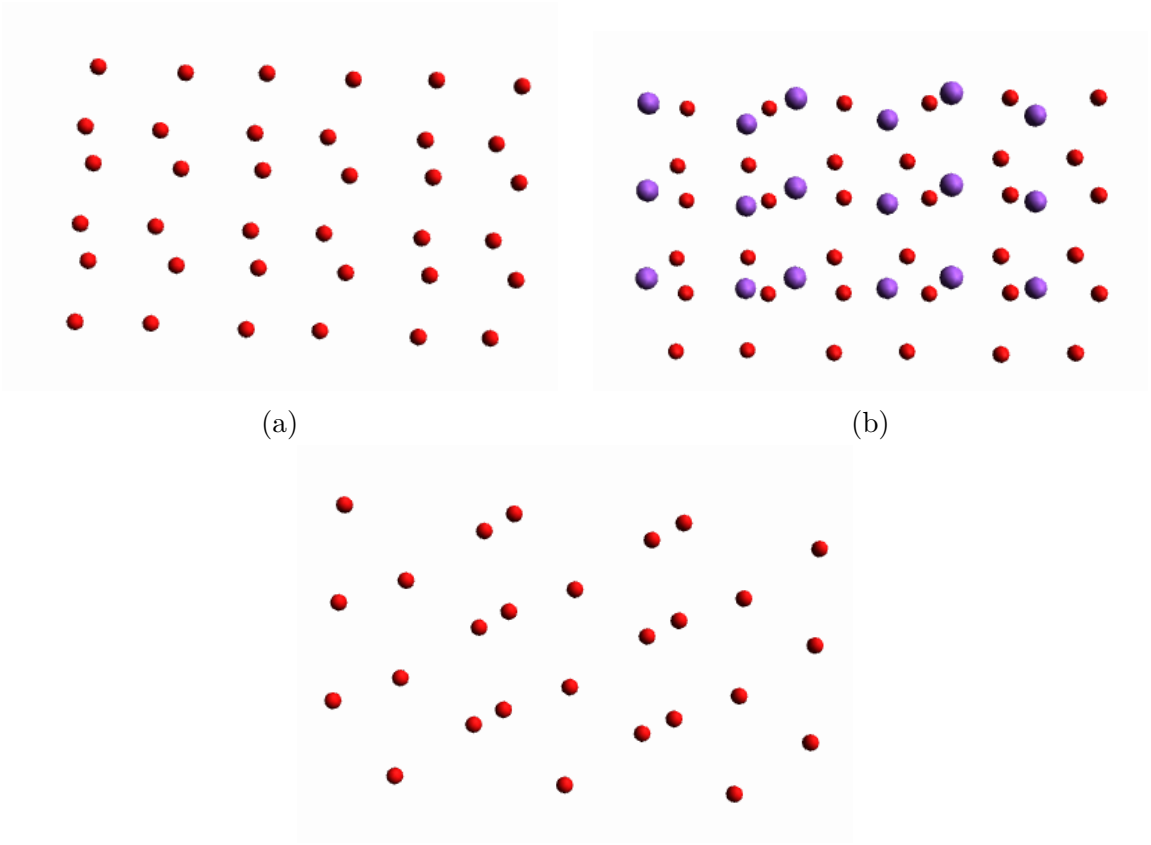

(a) (b)

(c)

Figure 4.11: Sodium-terminated mica slab with one water layer, showing (a) surface oxygens, (b) surface oxygens and Na^+ ions, and (c) water oxygens.

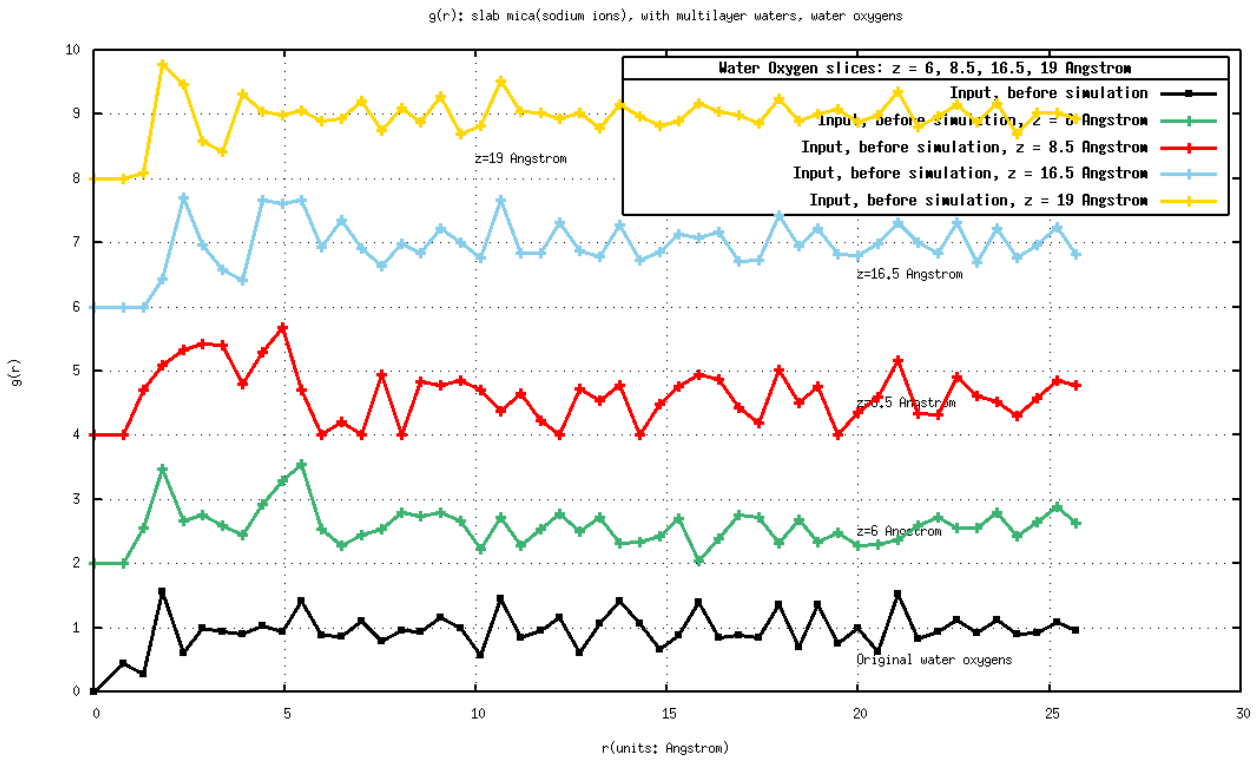

Figure 4.12: Two-dimensional pair correlation functions for water oxygens on a sodium-terminated mica slab with multiple water layers. The black line is from the original input structure. The other plots, offset for clarity, show pair correlation functions at the last step of the simulation for slices at z=6 Å (green), z=8.5 Å (red), z=16.5 Å (blue), and z=19 Å (yellow).

4.4.2 Na^+ Ions-terminated Mica Slab with Multiple Water Layers

Upon adding more water layers, there is a large increase in the width of the sodium ion "layer" which spreads into the water layers, with a width comparable to that seen for both the single and multiple water layer models with potassium. The effect of the sodium ions in structuring the multiple water layers is much weaker, as seen by the smaller and less distinct features in the pair correlation functions (Figure 4.12) for all water layers.

Model	Standard deviation in z (Å)
bulk mica	0.363
mica slab	0.077
mica slab, one H_2O layer	0.636
mica slab, multilayer H_2O	2.361

Table 4.5: Standard deviations (in Å) of Na^+ z coordinates for various models of sodiated mica after equilibration.

4.4.3 Additional Na^+ Ions within Water Layers on a Na^+-terminated Mica Slab

There is a different effect on water organization when adding more Na^+ ions in the water layers than there was in the K^+ case. The pair correlation functions for the water layers closest to the mica show less structure (fewer distinct peaks), while the inner layer with additional Na^+ ions shows the sharper peak at about 3 Å which was observed in the mica-adjacent layers for potassium. This is shown in Figure 4.13.

Therefore, the sodium ions show quite different behaviour than the potassium ions when water layers are added. The stronger anisotropy in the Na^+ models without water discussed in Chapter 3 does not translate in the models containing water.

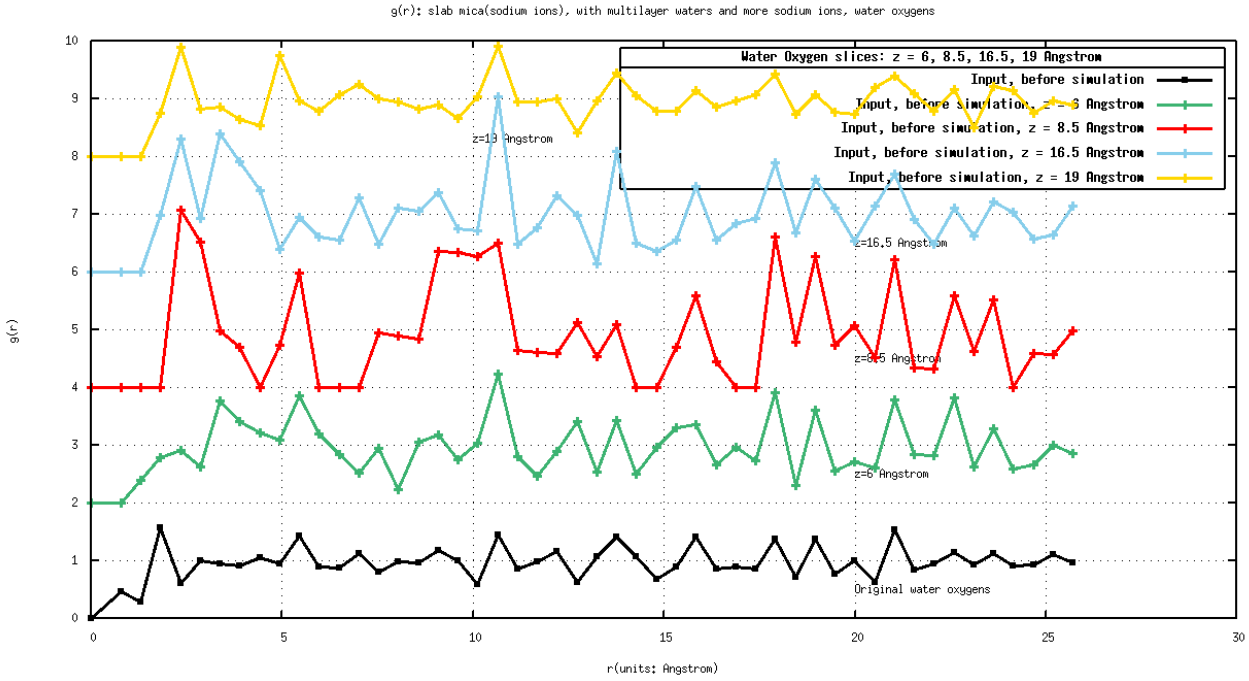

Figure 4.13: Two-dimensional pair correlation functions for water oxygens for the sodium-terminated mica slab with multiple water layers also containing sodium ions. The black line is from the original input structure. The other plots, offset for clarity, show pair correlation functions at the last step of the simulation for slices at z=6 Å (green), z=8.5 Å (red), z=16.5 Å (blue), and z=19 Å (yellow).

Chapter 5

Conclusions & Future Work

5.1 Conclusion

Experimentally, protein alignment was previously observed on the mica surface in register with underlying crystal directions. Here, molecular dynamics (MD) calculations were used to investigate whether the mica substrate affects ordering of the ions in fluid or environmental water. Our calculations show that ion arrangements on the mica surface play an important role in water pattern formation, and that the presence of water is important for ion rearrangement.

First, bulk mica was simulated. Based on the reasonable results for the mica alone (no unreasonable changes between the X-ray based input structure and the simulation output), that model was then used as the basis for adding and removing ions, creating a slab, and inserting waters. The changes in organization within a layer were analyzed using two dimensional pair correlation function calculations, with spreading of the layers within the structure measured with the standard deviation of the coordinates normal to the layer (z).

5.1.1 Comparison with Other Papers

Earlier Monte Carlo simulations [48, 49] showed the formation of a water layer influenced by and influencing the positions of adsorbed K^+ ions. Meleshyn's work [49] looked beyond films to observe the formation of larger water clusters whose position and shape were driven by K^+ ions in the vicinity of the mica surface.

Another article used Monte Carlo simulations to check liquid-solid interface phenomena: different ion-containing solutions were simulated with Cl^- surrounded muscovite mica [20]. The positive ions, H_3O^+ in particular, adsorb on the mica surface. X-ray reflectivity studies [50] show that the first adsorbed H_3O^+ layer approaches the K^+ ions. My simulations do not show significant migration of cations from solution to the cation layer; in contrast, there seems to be migration away from a tight layer adjacent to the aluminosilicate.

The difference between the behaviour of K^+ and Na^+ ions is interesting to note, since most prior simulations involving water and mica focus on K^+ cations only. MD simulations by Leng et al [51] show that water can co-adsorb with K^+ ions without entirely displacing them from the surface. These partially-hydrated K^+ ions are consistent with our findings on the K^+ systems with water. We see the displacement of ions for Na^+ as well, but the ions are not as readily displaced as the K^+ ions and require multiple layers of water to do so.

5.1.2 Comparison with experimental results on adsorbate ordering

The literature review in Chapter 1 presented several examples of ion-dependent aggregation and alignment. In the case of guanosine 5'-monophosphate (GMP) on mica, cations in solution do not seem to affect the formation of aligned aggregates, but the

researchers propose that the potassium ions from the mica surface play a significant role in alignment of adsorbates.[15] In contrast, the case of collagen aggregation and alignment on mica shows a strong dependence in aggregate morphology and quality of the alignment on the ions added to the solution (which may then adsorb onto the mica surface) [4].

My simulations show organization of the water above the surface for both K^+- and Na^+-containing systems. After the simulation, the waters which are closer to the ions form a more evenly spaced pattern. Interestingly the Na^+ ions have a stronger impact further from the mica surface.

The GMP work indicates that the potassium ions are required for aggregation, and without aggregation the alignment cannot occur. The GMP results also seem to imply that the potassium on the surface is sufficient to induce aggregation. My results support the observations from the collagen experiments, where the type of ion does make a difference and the sodium ions induce more organization in the layers above the mica surface. My simulations only reflect the organization of water molecules, but similar interactions (ion-dipole and hydrogen bonding) would play a role in the organization of collagen at or near the surface as well.

The interactions and alignment between the adsorbates and the mica is not just a matter of the mica inducing change in the solvated or suspended species. The surface layer(s) of the mica itself can undergo reconstruction. This was also addressed by my simulations, particularly looking at ion-dependence. As a baseline I deleted the cations from mica, but Al, Si and internal oxygen slices do not experience lots of changes in organization. When Na^+ ions were used to replace K^+ ions, the $g(r)$ plots for the Si and Al layers within the mica seem to show an expansion as peaks show up at larger r values.

Adding water layers did not reorder the surface oxygen layer of the mica (oxygen

slice at 13 Å) more than for runs where there was an empty gap, with or without the cation layer. When analyzing water organization (through the positions of the oxygens from the water), I studied water near the cation or slab interface (oxygens at e.g. 6 Å and 19.5 Å) and water further away from surface (e.g. 8.5 Å and 16.5Å). For the surface water the Na^+ systems showed more organization according to the pair correlation function, where stronger organizliational features (larger peaks) appeared for slices closer to the cation (Na^+) layers. The further water layers were connected by hydrogen bonding, with some translation of the structure.

5.2 Future Work

5.2.1 Mica, water and ions

There are many variants which could be studied in related systems. Chapters 3 and 4 show the results of K^+ and Na^+ ions with mica calculations. So, I wonder if I substitute K^+ ions or Na^+ ions with other ions with a different charge (such as Ca^{2+} or Fe^{3+}), whether the water would migrate and form a different pattern. Furthermore, there remains the question of whether adding in H^+ ions would produce similar trends.

5.2.2 Peptide Add-In

Experimentally, researchers put a collagen suspension on mica and found out that the mica-collagen systems interact with each other [4]. So far, ions play an important role for water pattering, but what about protein patterning?

For further calculations, a short peptide could replace some of the water. Observing peptide assembly computationally is quite complex even for short peptides [52, 53]. Larger peptides and proteins can be tackled using coarse-grained models [54] or periodic boundary conditions [55]. Adding in a surface makes things even more

complex, but simulations have been performed for short peptides adsorbing onto a range of surfaces including a short collagen-related peptide onto rutile [56]. Again, coarse-grained models can facilitate the process, allowing for larger proteins [57] or multiple proteins [58] to be studied.

5.2.3 Synchrotron Experiments

Synchrotron experiments can be used to measure the water-mica systems, obtaining atomic-level detail for comparison with the MD simulations [59].

X-ray diffraction (XRD) can be used to examine liquid-gas and liquid-solid interfaces [60]. Glancing angle X-ray diffraction (GAXRD), in particular, would be chosen due to the minimal contribution from the substrate and a good viewing for thin films.[61] In general for X-ray diffraction, the incidence angle should equal the diffracted beam angle. However, if the sample film is very thin and the incidence angle is quite large, highly intense beams might break through the sample film depth, which can give incorrect results. GAXRD gives configurations for incidence angles less than 10° as it is modified to provide a non-symmetric diffraction angle in order to enhance the sample results by minimizing the substrate contributions [62]. The glancing angle is changeable to allow depth profiling of the film [63].

For experiments analogous to my simulations, K^+ and Na^+ containing solutions would be prepared (with different concentrations), and mica would be immersed into the solutions [64]. Experiments would follow the computational methods, in order to match the results. In this way, the original mica, pure deionized water with mica, K^+ in water with mica, Na^+ in water with mica systems would be checked, with GAXRD data providing information about the arrangement of cations and mica surface oxygens under different conditions.

Bibliography

[1] Václav Štengl, Jan Šubrt, Snejana Bakardjieva, Andrea Kalendova, and Petr Kalenda. The preparation and characteristics of pigments based on mica coated with metal oxides. *Dyes and Pigments*, 58(3):239–244, 2003.

[2] F. Moreno-Herrero, J. Colchero, J. Gómez-Herrero, and A. M. Baró. Atomic force microscopy contact, tapping, and jumping modes for imaging biological samples in liquids. *Phys. Rev. E*, 69:031915, Mar 2004.

[3] D. M. Czajkowsky and Z. Shao. Inhibition of protein adsorption to muscovite mica by monovalent cations. *Journal of Microscopy*, 211(1):1–7, 2003.

[4] M. Sun, A. Stetco, and Erika F. Merschrod S. Surface-Templated Formation of Protein Microfibril Arrays. *Langmuir*, 24(doi : 10.1021/la703292h):5418–5421, 2008.

[5] Guven Necip. Mica Structure and Fibrous Growth of Illite. *Clays and Clay Minerals Society*, 49(3):189–196, 2001.

[6] Seung-gu Kang, Tien Huynh, Zhen Xia, Yi Zhang, Haiping Fang, Guanghong Wei, and Ruhong Zhou. Hydrophobic Interaction Drives Surface-Assisted Epitaxial Assembly of Amyloid-like Peptides. *Journal of the American Chemical Society*, 135(8):3150–3157, 2013.

[7] Yingguang Lin, Zhuoru Yang, Jiang Cheng, and Lianshi Wang. Synthesis, characterization and antibacterial property of strontium half and totally substituted hydroxyapatite nanoparticles. *Journal of Wuhan University of Technology-Mater. Sci. Ed.*, 23(4):475–479, 2008.

[8] James M. Helt and James D. Batteas. Wear of Mica under Aqueous Environments:Direct Observation of Defect Nucleation by AFM. *Langmuir*, 21:633–639, 2005.

[9] Werner Massa. *Crystal structure determination*, chapter 2. Springer, Berlin, 2004.

[10] Necip Güven. The crystal structures of 2 M_1 phengite and 2 M_1 muscovite. *Z Kristallogr.*, 134:196–212, 2010.

[11] Calvin F. Miller. Composition of plutonic muscovite: genetic implications. *Canadian Mineralogist*, 19:25–34, 1981.

[12] Bernhard Putsche, Levent Tumbek, and Adolf Winkler. The influence of potassium on the growth of ultra-thin films of para-hexaphenyl on muscovite mica(001). *J Chem Phys*, 137(13):134701, 2012.

[13] Sang Soo Lee, Paul Fenter, Kathryn L. Nagy, and Neil C. Sturchio. Monovalent ion adsorption at the muscovite (001)–solution interface: Relationships among ion coverage and speciation, interfacial water structure, and substrate relaxation. *Langmuir*, 28(23):8637–8650, 2012.

[14] Jacob N. Israelachvili, Norma A. Alcantar, Nobuo Maeda, Thomas E. Mates, and Marina Ruths. Preparing contamination-free mica substrates for surface characterization, force measurements, and imaging. *Langmuir*, 20(9):3616–3622, 2004.

[15] Klemen Kunstelj, Francesco Federiconi, Lea Spindler, and Irena Drevenšek-Olenik. Self-organization of guanosine 5'-monophosphate on mica. *Colloids and Surfaces B: Biointerfaces*, 59(2):120–127, 2007.

[16] Y Kuwahara. Muscovite surface structure imaged by fluid contact mode AFM. *Phys Chem. Minerals*, 26:198–205, 1999.

[17] Kevin M. Rosso, James R. Rustad, and Eric J. Bylaska. The Cs/K exchange in muscovite interlayers: an ab initio treatment. *Clays and Clay Minerals*, 49(6):500–513, 2001.

[18] Jianwei Wang, Andrey G. Kalinichev, R. James Kirkpatrick, and Randall T. Cygan. Structure, energetics, and dynamics of water adsorbed on the muscovite (001) surface: A molecular dynamics simulation. *J. Phys. Chem.*, B(109):15893–15905, 2005.

[19] Narasimhan Loganathan and Andrey G. Kalinichev. On the hydrogen bonding structure at the aqueous interface of ammonium-substituted mica: A molecular dynamics simulation. *Z. Naturforsch A*, 68:91–100, 2013.

[20] Artur Meleshyn. Aqueous Solution Structure at the Cleaved Mica Surface: Influence of K^+, H_3O^+, and Cs^+ Adsorption. *J Phys Chem C*, 112(50):20018–20026, 2008.

[21] Hui Li and Xiao Cheng Zeng. Two dimensional epitaxial water adlayer on mica with graphene coating: An ab initio molecular dynamics study. *Journal of Chemical Theory and Computation*, 8(9):3034–3043, 2012.

[22] Jeff A. Hughes. *The Manhattan Project: big science and the atom bomb*. Columbia University Press, first edition, 2002.

[23] Daan Frenkel and Berend Smit. *Understanding Molecular Simulation: From Algorithms to Applications*. Computational science series. Academic Press, San Diego, second edition, 2001.

[24] G. Makov and M. C. Payne. Periodic boundary conditions in ab initio calculations. *Phys. Rev. B*, 51(7):4014–4022, 15 February 1995.

[25] A. T. Hagler, S. Lifson, and P. Dauber. Consistent force field studies of intermolecular forces in hydrogen bonded crystals. II. A benchmark for the objective comparison of alternative force fields. *J. Am. Chem. Soc.*, 101:5122–5130, 1979.

[26] Hendrik Heinz, R. A. Vaia, R. Krishnamoorti, and B. L. Farmer. Self-assembly of alkylammonium chains on montmorillonite: effect of chain length, head group structure, and cation exchange capacity. *Chemistry of Materials*, 19(1):59–68, 2007.

[27] H. Q. Ding, N. Karasawa, and W. A. Goddard. Atomic level simulations on a million particles: The cell multipole method for Coulomb and London nonbond interactions. *J. Chem. Phys.*, 97:4309–4315, 1992.

[28] Linus Pauling. *The Nature of the Chemical Bond and the Structure of Molecules and Crystals: An Introduction to Modern Structural Chemistry*. George Fisher Baker Non-Resident Lecture Series. Cornell University Press, Ithaca, NY, third edition, 1960.

[29] V. A. Parsegian. *Van der Waals Forces: A Handbook for Biologists, Chemists, Engineers, and Physicists*. Cambridge University Press, 2006.

[30] A Warshel and J Aqvist. Electrostatic energy and macromolecular function. *Annual Review of Biophysics and Biophysical Chemistry*, 20(1):267–298, 1991. PMID: 1714279.

[31] T. Clark. *A handbook of computational chemistry: a practical guide to chemical structure and energy calculations*. A Wiley Interscience publication. Wiley, 1985.

[32] Steve Plimpton. Fast parallel algorithms for short-range molecular dynamics. *Journal of Computational Physics*, 117(1):1–19, 1995.

[33] Accelrys Software Inc., Discovery Studio Modelling Environment, Release 4.0, San Diego: Accelrys Software Inc., 2013.

[34] Paul D Lyne. Structure-based virtual screening: an overview. *Drug Discovery Today*, 7(20):1047–1055, 2002.

[35] Hendrik Heinz, Hilmar Koerner, Kelly L. Anderson, Richard A. Vaia, and B. L. Farmer. Force field for mica-type silicates and dynamics of octadecylammonium chains grafted to montmorillonite. *Chemistry of Materials*, 17(23):5658–5669, 2005.

[36] David A. McKeown, Michael I. Bell, and Edgar S. Etz. Raman spectra and vibrational analysis of the trioctahedral mica phlogopite. *American Mineralogist*, 84(5-6):970–976, 1999.

[37] Glenn J. Martyna, Michael L. Klein, and Mark Tuckerman. Nosé-Hoover chains: The canonical ensemble via continuous dynamics. *J Chem Phys*, 97(4):2635–2643, 1992.

[38] Ju Li. AtomEye: an efficient atomistic configuration viewer. *Modelling and Simulation in Materials Science and Engineering*, 11(2):173, 2003.

[39] Marcus Hanwell, Donald Curtis, David Lonie, Tim Vandermeersch, Eva Zurek, and Geoffrey Hutchison. Avogadro: an advanced semantic chemical editor, visualization, and analysis platform. *Journal of Cheminformatics*, 4(1):17, 2012.

[40] E Katchalski-Katzir, I Shariv, M Eisenstein, A A Friesem, C Aflalo, and I A Vakser. Molecular surface recognition: determination of geometric fit between proteins and their ligands by correlation techniques. *Proceedings of the National Academy of Sciences*, 89(6):2195–2199, 1992.

[41] Alan K. Soper and Maria Antonietta Ricci. Structures of high-density and low-density water. *Phys. Rev. Lett.*, 84:2881–2884, Mar 2000.

[42] Richard W. Loo and M. Cynthia Goh. Potassium Ion Mediated Collagen Microfibril Assembly on Mica. *Langmuir*, 24(23):13276–13278, 2008.

[43] Carlo A. Rozzi, Daniele Varsano, Andrea Marini, Eberhard K. U. Gross, and Angel Rubio. Exact coulomb cutoff technique for supercell calculations. *Phys. Rev. B*, 73:205119, May 2006.

[44] Fukuda Ikuo, Yasushige Yonezawa, and Haruki Nakamura. Molecular dynamics scheme for precise estimation of electrostatic interaction via zero- dipole summation principle. *J. Chem. Phys.*, 134:164107, April 2011.

[45] Céline Anézo, Alex H. de Vries, Hans-Dieter Höltje, D. Peter Tieleman, and Siewert-Jan Marrink. Methodological issues in lipid bilayer simulations. *J. Phys. Chem. B.*, 107:9424–9433, June 2003.

[46] Kenjiro Oura. *Surface science : an introduction.* Advanced texts in physics. Springer, Berlin ; New York, 2003.

[47] L. Cheng, P. Fenter, K. L. Nagy, M. L. Schlegel, and N. C. Sturchio. Molecular-scale density oscillations in water adjacent to a mica surface. *Phys. Rev. Lett.*, 87:156103, Sep 2001.

[48] Sung-Ho Park and Garrison Sposito. Structure of water adsorbed on a mica surface. *Phys. Rev. Lett.*, 89:085501, Aug 2002.

[49] Artur Meleshyn. Two-dimensional ordering of water adsorbed on a mica surface at room temperature. *The Journal of Physical Chemistry C*, 112(37):14495–14500, 2008.

[50] Hiroshi Sakuma, Hironori Nakao, Yuichi Yamasaki, and Katsuyuki Kawamura. Structure of Electrical Double Layer at Mica/KI Solution Interface. *Journal of Applied Solution Chemistry and Modeling*, 1:1–5, 2012.

[51] Yongsheng Leng and Peter T. Cummings. Hydration structure of water confined between mica surfaces. *J Chem Phys*, 124(7):074711, 2006.

[52] Davide M. Marini, Wonmuk Hwang, Douglas A. Lauffenburger, Shuguang Zhang, and Roger D. Kamm. Left-handed helical ribbon intermediates in the self-assembly of a β-sheet peptide. *Nano Letters*, 2(4):295–299, 2002.

[53] Ernesto Suárez, Natalia Díaz, and Dimas Suárez. Entropic control of the relative stability of triple-helical collagen peptide models. *J Phys Chem B*, 112(47):15248–15255, 2008.

[54] Marieke Schor, Bernd Ensing, and Peter G. Bolhuis. A simple coarse-grained model for self-assembling silk-like protein fibers. *Faraday Discuss.*, 144:127–141, 2010.

[55] Ian Streeter and Nora H. de Leeuw. Atomistic modeling of collagen proteins in their fibrillar environment. *J Phys Chem B*, 114(41):13263–13270, 2010.

[56] Ting Zheng, Chunya Wu, and Mingjun Chen. Early adsorption of collagen on the reduced rutile (110) surface mediated by water: A molecular dynamics study. *Surface Science*, 616:51–59, 2013.

[57] Shuai Wei and Thomas A. Knotts. A coarse grain model for protein-surface interactions. *J Chem Phys*, 139(9):095102, 2013.

[58] R. B. Pandey and B. L. Farmer. Distinction in binding of peptides (P2E) and its mutations (P2G, P2Q) to a graphene sheet via a hierarchical coarse-grained Monte Carlo simulation. *The Journal of Chemical Physics*, 139(16):164901, 2013.

[59] F. R. Elder, A. M. Gurewitsch, R. V. Langmuir, and H. C. Pollock. Radiation from electrons in a synchrotron. *Phys. Rev.*, 71:829–830, Jun 1947.

[60] Y. Fukushima. X-Ray Diffraction Study of Aqueous Montmorillonite Emulsions. *Clays and Clay Minerals*, 32:320–326, 1984.

[61] Mirtat Bouroushian and Tatjana Kosanovic. Characterization of Thin Films by Low Incidence X-Ray Diffraction. *Crystal Structure Theory and Applications*, 1:35–39, 2012.

[62] Hirotaka Ohashi, Katsumi Tanigaki, Ryotaro Kumashiro, Syuji Sugihara, Shinya Hiroshiba, Shigeru Kimura, Kenichi Kato, and Masaki Takata. Low-glancing-angle x-ray diffraction study on the relationship between crystallinity and properties of C_{60} field effect transistor. *Applied Physics Letters*, 84(4):520–522, 2004.

[63] Paolo Colombi, Paolo Zanola, Elza Bontempi, Roberto Roberti, Marcello Gelfi, and Laura E. Depero. Glancing-incidence X-ray diffraction for depth profiling of polycrystalline layers. *Journal of Applied Crystallography*, 39(2):176–179, Apr 2006.

[64] Hiroshi Sakuma, Toshihiro Kondo, Hironori Nakao, Koichi Shiraki, and Katsuyuki Kawamura. Structure of hydrated sodium ions and water molecules adsorbed on the mica/water interface. *J Phys Chem C*, 115(32):15959–15964, 2011.

Appendix A

Simulation Scripts

A.1 ".car" & ".mdf" Geometry Files

A.1.1 ".car" File Format

```
PBC=ON
PBC    5.1918    9.0153   20.0457   90.0000   95.7350   90.0000 (P1)
AL1      1.298828125    0.752777576    0.001595629 XXX  1      ay1     Al  1.449
SI1      2.140627623    8.376114845    2.703195333 XXX  1      sy1     Si  1.100
SI2      2.073014021    2.326848984    2.704392195 XXX  1      sy2     Si  1.100
K1      -0.500779569    0.883499384    4.986341476 XXX  1      k+      K   1.000
H1       1.814997077    5.859043598    1.194727421 XXX  1      hoy     H   0.200
O1       1.826298237    0.835718334    3.356805086 XXX  1      oy1     O  -0.550
O2       0.984393775    7.308703899    3.147977114 XXX  1      oy2     O  -0.550
.........................
.........................
end
end
```

A.1.2 ".mdf" File Format

```
#topology
@column 1 element
@column 2 atom_type
@column 3 charge_group
@column 4 isotope
@column 5 formal_charge
@column 6 charge
@column 7 switching_atom
@column 8 oop_flag
@column 9 chirality_flag
@column 10 occupancy
@column 11 xray_temp_factor
@column 12 connections
@molecule MICA_UNITCELL
XXX_1:AL1 Al ay1 ?  0  3+    1.4490 0 0 8 1.0000  0.0000 O5 O41%00-1#1 O16%00-1#1 ...
XXX_1:SI1 Si sy1 ?  0  0     1.1000 0 0 8 1.0000  0.0000 O4 O2 O27 O1%010#1
XXX_1:SI2 Si sy2 ?  0  0     1.1000 0 0 8 1.0000  0.0000 O5 O1 O3 O26
XXX_1:K1  K  k+  ?  0  1+    1.0000 0 0 8 1.0000  0.0000
XXX_1:H1  H  hoy ?  0  0     0.2000 0 0 8 1.0000  0.0000 O6
XXX_1:O1  O  oy1 ?  0  0    -0.5500 0 0 8 1.0000  0.0000 SI2 SI1%0-10#1
XXX_1:O2  O  oy2 ?  0  0    -0.5500 0 0 8 1.0000  0.0000 SI1 SI10%-100#1
XXX_1:O12 O  oy9 ?  0  1-   -0.6830 0 0 8 1.0000  0.0000 H2 AL8 AL6
.........................
.........................
!
#symmetry
```

```
@periodicity 3 xyz

@group (P1)

#end
```

A.2 Force Field (cvff_phyllosilicates) File Format

```
!Ver  Ref  Function Label

!---- ---   ---------------------------------------

 2.0  18    atom_types        cvff

 1.0   1    equivalence       cvff

 2.0  18    auto_equivalence  cvff_auto

 1.0   1    hbond_definition  cvff

 2.0  18    morse_bond        cvff   cvff_auto

 2.0  18    quadratic_angle   cvff   cvff_auto

 2.0  18    torsion_1         cvff   cvff_auto

 2.0  18    out_of_plane      cvff   cvff_auto

 1.0   1    nonbond(12-6)     cvff

 2.0  18    bond_increments   cvff

..........

> Atom type definitions for any variant of cvff

> Masses from CRC 1973/74 pages B-250.

!Ver  Ref  Type    Mass      Element  Connections   Comment

!---- ---  ----  ----------  -------  ----------------------------------------

 3.2  24    nac+  22.989800    Na          1        Sodium ion in Clays

 3.4  30    koh   39.098300    K           1        Potassium ion in water

 .........

> Equivalence table for any variant of cvff

!             Equivalences
```

```
!                 ----------------------------------------
!Ver  Ref   Type  NonB     Bond    Angle    Torsion    OOP
!---- ---   ----  ----     ----    -----    -------    ----
 3.1  30    li+   li+      li+      li+      li+       li+
 1.0   1    h     h        h        h        h         h
 1.0   1    d     h        h        h        h         h
 1.0   1    hp    h        h        h        h         h
..........
```

A.3 Run Script for Generating LAMMPS Data File: lammps05

```
 export BIOSYM_LIBRARY=user directory
../src/msi2lmp.exe filename -class I -frc cvff_phyllosilicates
 > data.filename_cvff_phy
```

A.4 LAMMPS Input Script

```
#Lammps input file for mica sheet
#Created by Muyi Xu
# ---------------- Initialization --------------------
clear
units real
dimension 3
boundary p p p
newton on
atom_style full
atom_modify map array
```

```
#---------------- Force Field  ----------------
pair_style coul/cut 2.5
bond_style harmonic
angle_style harmonic
dihedral_style harmonic
improper_style  cvff
special_bonds lj/coul 0.0 0.0 0.5
#----------------- Read Data File ---------------------
read_data bulkmica.lammps05
neighbor 1.2 bin
..........
# --------------- Atom definition ---------------------
replicate 1 1 1
# ---------- Settings --------------------
compute 1 all bond/local dist eng
compute eng all pe/atom
compute eatoms all reduce sum c_eng
compute 2 all property/atom xs ys zs vx vy vz
# ---------- Run Simulation ---------------------
reset_timestep 0
timestep 0.00005
velocity all create 300 12345 mom yes rot no
fix 1 all npt temp 300 300 1 iso 0 0 100 drag 1
#thermo commands
thermo 10
thermo_style custom step temp pe lx ly lz etotal press pxx pyy pzz
thermo_modify lost ignore
run 20000
```

```
unfix 1
variable tmp equal "lx"
variable L0 equal ${tmp}
print "Initial Length, L0: ${L0}"
reset_timestep 0
timestep 0.0001
.......
fix 1 all npt temp 300.0 300.0 10.0 iso 0.0 0.0 100.0 drag 0.5
variable srate equal 1.0e10
variable srate1 equal "-v_srate / 1.0e12"
# Output strain and stress info to file
# for units metal, pressure is in [bars] = 100 [kPa] = 1/10000 [GPa]
# p2, p3, p4 are in GPa
variable strain equal "(lx - v_L0)/v_L0"
variable p1 equal "v_strain"
variable p2 equal "-pxx/10000"
variable p3 equal "-pyy/10000"
variable p4 equal "-pzz/10000"
fix def1 all print 100 "${p1} ${p2} ${p3} ${p4}" file mica_comp_100.def1.txt
variable natoms equal "count(all)"
variable teng equal "c_eatoms"
variable length equal "lx"
variable ecoh equal "v_teng/v_natoms"
dump 1 all cfg 250 dump.comp_*.cfg id type xs ys zs id type vx vy vz
thermo 10
thermo_style custom step v_strain temp v_p2 v_p3 v_p4 ke pe press
run 10000
print "All done!"
```

A.5 Run Script for LAMMPS Input Script

```
#$ -cwd

#$ -l h_rt=48:00:00

module purge

module load intel openmpi/intel lammps

mpirun lammps < filename.in
```

Appendix B

Finite Temperature Check

B.1 LAMMPS Input: Set up for Temperature

In my LAMMPS input file, I set the temperature using the following command:

"fix 1 all npt temp 300.0 300.0 10.0 iso 0.0 0.0 100.0 drag 0.5 "

which allows me to start and stop the temperature at 300 K, under "NPT" conditions (refer to Chapter 2, section 2.2.2, "LAMMPS Input Script & Simulation Set Up".)

In order to make sure the simulation is reasonable for the real world case, the temperature during the simulation was checked. It is necessary to make sure that the temperature would not become extremely high during the run. The results are shown in Figure B.1.

Following the initial run of 20,000 steps, I restarted the simulation using the final step in the original output file as the starting point for the new input file, running for another 10,000 steps. Then I restarted the simulation using the last step of the previous run as the starting point for the new one, running for another 20,000 steps.

Below are the figures showing the temperatures for original 20,000-step simulation (Figure B.1 (a)) and for the following 10,000 steps (b) and the final 20,000 steps (c). The temperatures all stop around 300 K and with more calculation steps, the temperature fluctuations show similar magnitudes around the equilibrium temperature (300 K). The final

structure after 50,000 steps shows a nearly identical geometry to that after 10,000 steps, with the same pair-correlation functions for various layers averaged over the final steps as for the equilibrium steps nearing 10,000.

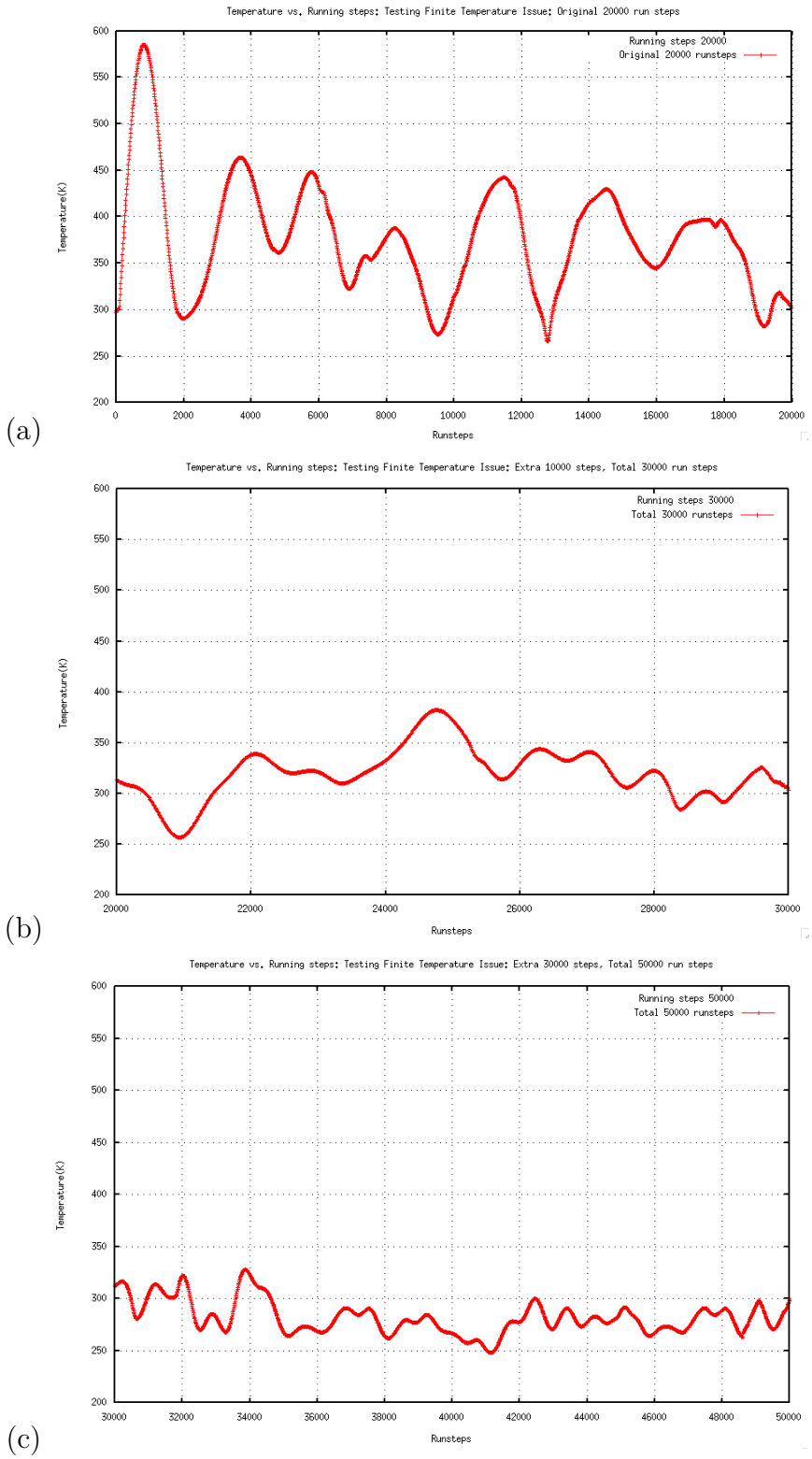

Figure B.1: Temperature vs. steps for (a) the original simulation, (b) a subsequent simulation with 10,000 steps, and (c) a following simulation with 20,000 steps. The vertical scales (temperature) are the same for all three plots, while the horizontal scales vary.

Appendix C

L-J Potential Check

In Chapter 1, I mentioned that a general form for inter-particle interactions is the Lennard-Jones potential: [23]

$$f(r) = \frac{48\epsilon}{r^2}\left(\frac{1}{r^{12}} - 0.5\frac{1}{r^6}\right) \tag{C.1}$$

where ϵ represents the strength of the interaction and r is the distance between particles.

The cut-off energy e_{cut} beyond which interactions are neglected is the potential at $r = r_c$.

In my simulation, I used 2.5 Å as a cut-off distance and below I plot a general example to check whether the set up L-J potential is reasonable for my calculation. The parameter ϵ is obtained from the force field file. I chose mica oxygens to check the L-J potential plot's shape, and ϵ_{Oxygen} is 1. The plot turns flat around the cut-off distance, 2.5Å, which means my cut-off distance would not effect my calculation accuracy.

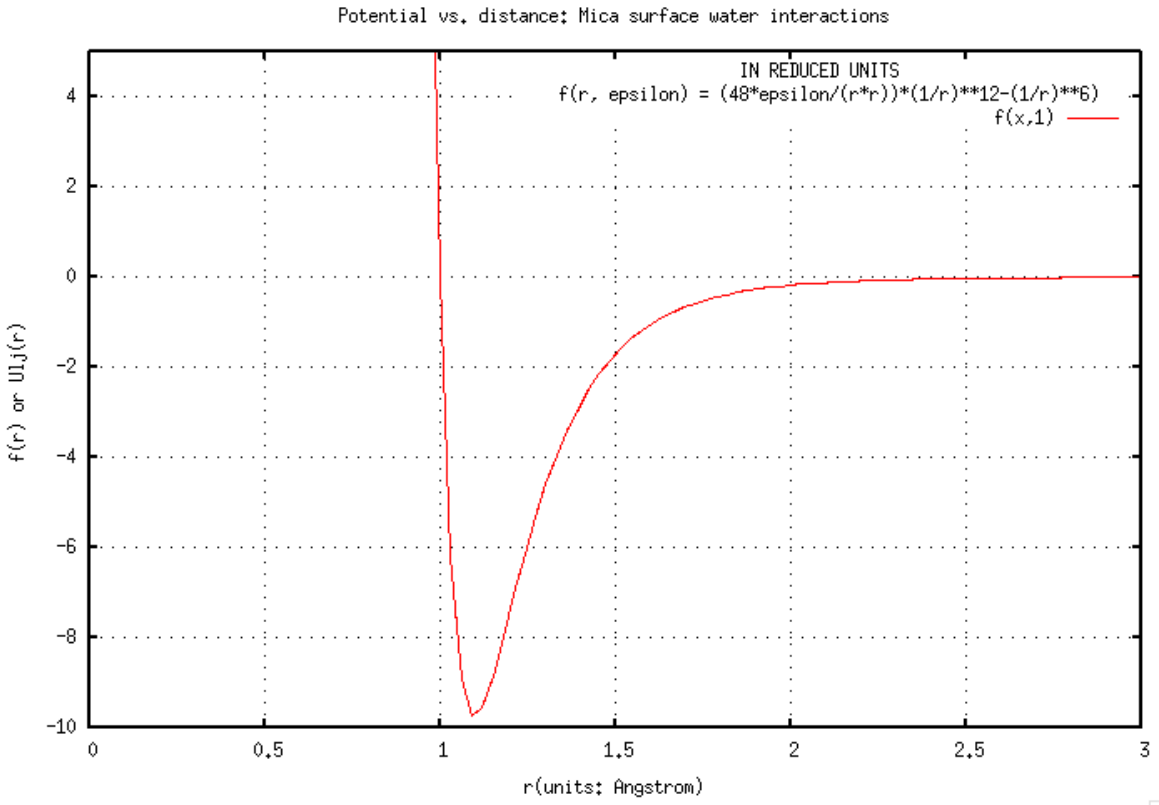

Figure C.1: Oxygen-oxygen potential *vs* distance plot($\epsilon_O = 1$).